Khosravi, Ali; Syri, Sanna

Modeling of Geothermal Power System Equipped with Absorption Refrigeration and Solar Energy using Multilayer Perceptron Neural Network Optimized with Imperialist Competitive Algorithm

Published in:
Journal of Cleaner Production

DOI:
10.1016/j.jclepro.2020.124216

Published: 10/12/2020

Document Version
Peer-reviewed accepted author manuscript, also known as Final accepted manuscript or Post-print

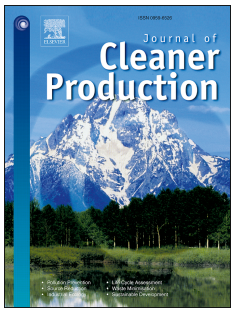

Modeling of Geothermal Power System Equipped with Absorption Refrigeration and Solar Energy using Multilayer Perceptron Neural Network Optimized with Imperialist Competitive Algorithm

A. Khosravi, S. Syri

PII: S0959-6526(20)34261-X

DOI: https://doi.org/10.1016/j.jclepro.2020.124216

Reference: JCLP 124216

To appear in: *Journal of Cleaner Production*

Received Date: 10 April 2019

Revised Date: 2 September 2020

Accepted Date: 13 September 2020

Please cite this article as: Khosravi A, Syri S, Modeling of Geothermal Power System Equipped with Absorption Refrigeration and Solar Energy using Multilayer Perceptron Neural Network Optimized with Imperialist Competitive Algorithm, *Journal of Cleaner Production*, https://doi.org/10.1016/j.jclepro.2020.124216.

CRediT statements

Ali Khosravi: Conceptualization, Methods, Data gathering, Software, Investigation, Writing- Original draft preparation, Validation, Visualization.

Sanna Syri*:* Conceptualization, Supervision, Visualization, Reviewing and Editing, Project administration, Funding acquisition.

Modeling of Geothermal Power System Equipped with Absorption Refrigeration and Solar Energy using Multilayer Perceptron Neural Network Optimized with Imperialist Competitive Algorithm

A. Khosravi*, S. Syri

Department of Mechanical Engineering, School of Engineering, Aalto University, Helsinki, Finland

*Corresponding author: Ali Khosravi
Postdoctoral Researcher
Aalto University
Department of Mechanical Engineering, Group of Energy Efficiency and Systems
Otakaari 4 Espoo 1.kerros 157b
Helsinki, Finland
Email: ali.khosravi@aalto.fi, Alikhosravii@yahoo.com
Tel: +358 41 7234958

Modeling of Geothermal Power System Equipped with Absorption Refrigeration and Solar Energy using Multilayer Perceptron Neural Network Optimized with Imperialist Competitive Algorithm

A. Khosravi*, S. Syri

Department of Mechanical Engineering, School of Engineering, Aalto University, Helsinki, Finland
* Corresponding author: Ali.khosravi@aalto.fi

Abstract

For geothermal energy system, the low geothermal well operating lifetime and temperature is one of the main obstacles. Also, finding the optimum design parameters and operating conditions requires many experimental tests and intricate mathematical models. Besides, improving the energy efficiency and lacking technical feasibility of the combined geothermal systems are other challenges concerning geothermal systems. To cover the mentioned challenges, in the current study, a hybrid geothermal/absorption refrigeration system (ARS) incorporated with solar thermal collector, desalination unit and hydrogen storage system is designed and assessed. The proposed system is investigated by developing two methods of artificial intelligence (AI) as well as thermodynamic model. The intelligent methods are multilayer perceptron (MLP) neural network optimized with imperialist competitive algorithm (ICA), MLP-ICA, and MLP optimized with genetic algorithm (GA), MLP-GA. These methods are manufactured based on the solar irradiance, cooling water temperature difference, ambient temperature, pinch-point temperature, evaporating and condensing temperatures as independent parameters. These parameters are utilized to obtain the power generation, coefficient of performance of the ARS ($COP_{chiller}$), heat exchanger area of the ARS, and cycle thermal efficiency.

The obtained results show that simulation of the system by MLP-ICA was successfully carried out and this model operates substantially better than the MLP-GA for simulating the behavior of the system. Also, the payback time for the proposed system (with the interest rate of 3%) was obtained around 8 years.

Keywords: Geothermal energy system; Absorption refrigeration system; Solar thermal collector; Desalination unit; Imperialist competitive algorithm; Genetic algorithm

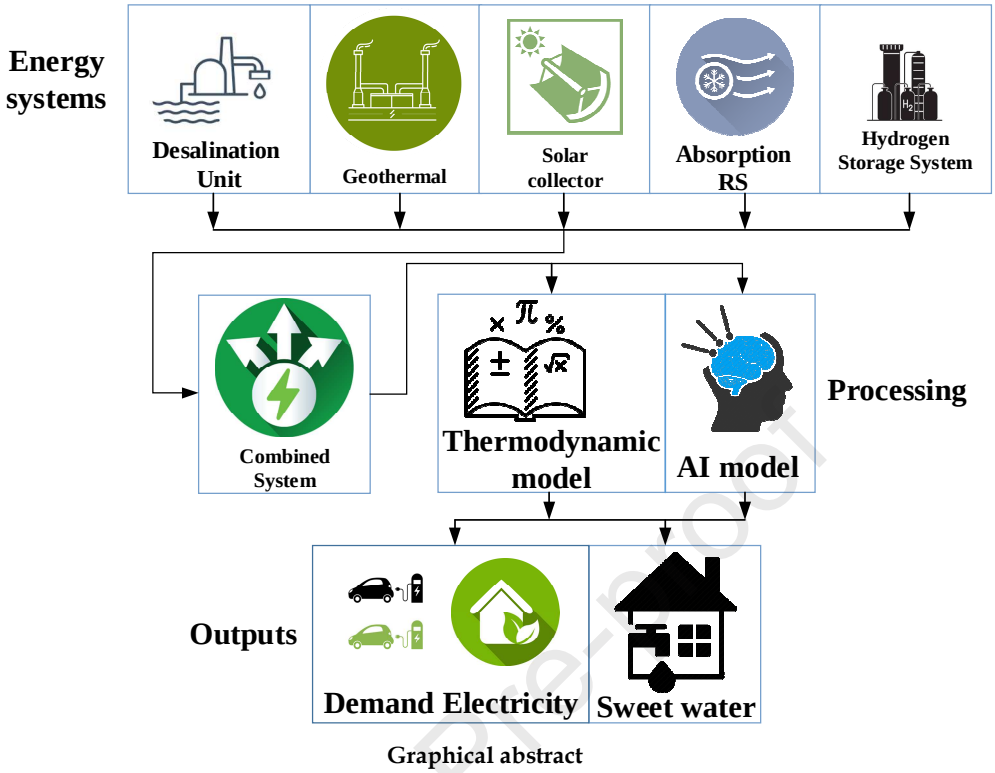

Graphical abstract

1. Introduction

Renewable energy (RE) resources due to the increased awareness of harmful effects of fossil fuels on the earth, its climate and the health of its inhabitants have been considered as an alternative for energy sources [1]. Geothermal energy (GE) is an incessant source of energy that is a remarkable feature for developing an energy system compared to the other renewable resources such as solar and wind [2], [3]. GE can be utilized either directly or indirectly in many energy systems. Commonly, for extracting the steam from liquid in geothermal fluid mixtures, a separation process is applied. During the separation process, low-grade thermal energy is produced, which is considered a wasted energy source [4]. This low-grade thermal energy is recycled in many engineering applications like district heating and cooling, power generation and drying. Commonly, for producing cooling, for instance in compression refrigeration system, compressor consumes electrical energy for compression process [5]. Absorption refrigeration system (ARS) is a cooling system, which requires a heat source in the generator as the input energy. Hence, this system is used as a combined system with the geothermal system in order to use the wasted low-grade thermal energy [6].

Several investigations have been developed to employ GE in various energy applications. [7] designed a geothermal heat pump (GHP) to supply the cooling demand of telecommunications data center. The GHP system was compared to air-source heat pump (ASHP) cooling system. They achieved that the GHP system operated better than the ASHP from energy and economic point of views. [8] exerted geothermal technology to energy recovery from deep flooded copper mines for a heating application. Their analysis has shown that the annual extractable energy from the mentioned energy resource can support over 82,000 households that is analogous to the annual

energy produced by a small-scale power station. Geothermal heating and cooling systems were evaluated by [9]. They discussed on district energy systems, combination of GE system with other energy conversion systems for supplying cooling and heating. A combination of power and water system with cascade GE was investigated by [10]. A thermodynamic simulation to evaluate the proposed system through energy, exergy and economic assessments was developed. It was shown that when the evaporation temperature increased, the thermodynamic performance, as well as the relevant cost of the combined system, enhanced.

Nomenclature

A: area (m^2)
c_p: specific heat (kJ/kg K)
g: acceleration of gravity (m/s^2)
h: enthalpy (kJ/kg)
i_r: interest rate
LHV: lower heating value (kJ/kg)
$LMTD$: logarithmic mean temperature difference (℃)
$\dot{m}$: mass flow rate (kg/s)
MW_w: molar mass of water (kg/kmol)
n_p: project lifetime
P: pressure (kPa)
$\dot{Q}$: heat transfer rate (kW)
T: temperature ℃
$\dot{W}$: work rate (kW)
$\dot{W}_t$: power output of the turbine (kW)
X: solubility
x: quality of vapor

Greek Symbols

ρ: density (kg/m^3)
η: efficiency
$\dot{v}$: volumetric flow rate (m^3/s)
μ: dynamic viscosity (pa.s)
v: specific volume (m3/kg)

Abbreviations

ANN: artificial neural network
ANFIS: adaptive neuro-fuzzy inference system
AI: artificial intelligence
ARS: absorption refrigeration system
CC: Capital cost
FIS: Fuzzy inference system
GA: genetic algorithm
GMDH: Group method of data handling
H_2: hydrogen
IC: installation cost
ICA: imperialist competitive algorithm
IAPWS: water and steam
LCOE: levelized cost of energy
LCC: life cycle cost
MLP: multilayer perceptron
MC: maintenance cost
NaCl: salt
O_2: oxygen
PSO: Particle swarm optimization
RBF: radial basis function
RES: Renewable energy system
RC: replacement cost
R.HX=refrigeration heat exchanger
SVR: support vector regression
S.HX= solution heat exchanger

Subscripts/Superscripts

a: absorber
cond: condenser
cryst: cristalization
eva: evaporator
FW: feed water
g: generator
in: input
libr: lithium bromide
out: output
p: pump
sat: saturation
sc: solar collector
t: turbine
w: water
wf: working fluid

[11] designed an energy supply system for providing cooling, heating and electrical power simultaneously (CCHP). The combined system was a combination of biomass, geothermal and natural gas. They presented that considering natural gas as an auxiliary system enhances energy efficiency and remarkably decreases the levelized cost of energy (LCOE). [12] presented a hybrid geothermal-based system for supplying hot water, heating, hydrogen production, electrical power, and oxygen simultaneously. They investigated the impacts of evaporator temperature of absorption chiller, geothermal well temperature, pinch-point temperature and turbine input pressure over the performance of the hybrid system. It was determined that the overall energy and exergy efficiencies were 42.59%

and 48.24%, consecutively. Moreover, the other research projects regarding GE systems are as follows: [13] appraised the efficiency of a low-temperature geothermal system incorporated with freshwater production unit in an island area. [14] assessed conventional and unconventional deep geothermal well concepts. [15] employed thermodynamic and economic analyses for assessing the comparison-absorption cascade refrigeration system powered by GE. [16] proposed ARS as an auxiliary cooling system for a GE system. [17] propounded a hybrid system working with geothermal resource for producing the electrical power and freshwater simultaneously. A similar study also was developed by [18] in which GE was employed for generating electrical power and freshwater.

Recently, many research projects have been presented to show the impress of energy storage systems to scheme and develop more efficient energy systems for different geographical and meteorological conditions. More specifically, RE sources comprising solar and wind are highly fluctuating. Hence, energy storage system in RE sector is inevitable. It is particularly significant in the case of solar, wind, ocean thermal and tidal to ensure availability of electricity throughout the year. Among the energy storage systems, hydrogen storage system has been proposed especially for the large-scale RESs. In most cases, hydrogen storage was adapted for the hybrid photovoltaic/wind turbine as an energy storage unit [19], [20].

Since ancient times, the feasibility of introducing and developing a system that would “think” has been of interest to scholars. Artificial intelligence (AI) have been widely utilized in energy engineering systems. [21] implemented an artificial neural network (ANN) for forecasting the produced power by a photovoltaic system. It was found out that the observed error between the measured data and estimated data by ANN was about 0.5-9%. [22] developed an intelligent method through combination of ANN inverse with genetic algorithm (GA) to simulate an absorption heat transformer system for finding the optimal multivariable conditions. [23] utilized an ANN for modeling of the household energy consumptions. [24] for prediction of wind speed and electrical power output of a wind turbine compared the performance prediction of three intelligent methods comprising ANN, ANFIS and SVR. It was obtained that the predicted data by the SVR are better than ANN and ANFIS. The hybrid ANFIS-PSO and ANFIS-GA methods were implemented for forecasting the wind speed in Osorio wind farm, Brazil [25]. In other studies, ANFIS-PSO, ANFIS-GA, ANFIS-AC (ANFIS-optimized with ant colony), ANN, SVR, GMDH, RBF neural network and FIS (fuzzy inference system) have been implemented to estimate solar radiation [26], [27]. [26] expressed that incorporating the optimization methods with conventional intelligent methods enhances the prediction performance in intricate prediction problems.

1.1. Contribution of this study

The main purpose of this research is to demonstrate how AI methods simulate RESs and catch the hidden pattern between the input parameters and targets. The current study presents a concept of how intelligent methods will employ to find the best operating conditions, performance evaluation and power generation prediction for a hybrid system. For this target, two hybrid methods of AI implemented based on machine learning algorithms to simulate the manner of the hybrid geothermal/ARS incorporated with solar thermal system. The intelligent methods are multilayer perceptron (MLP) neural network combined with imperialist competitive algorithm (ICA), (MLP-ICA), and MLP combined with genetic algorithm (GA), MLP-GA. In spite of many studies on ANN applied for modeling

of energy systems, no study has yet been reported in the literature on examining the efficiency of the proposed hybrid methods (MLP-ICA and MLP-GA). On the other hand, investigations have shown that 1.2 billion people have little or no access to electricity. Also, one shocking similarity in this large number is the urban-rural division. Upwards of 80 percent of sufferers of energy-poverty live in rural or remote areas. This study proposes a new combination of RESs for supplying the power demand and producing the freshwater, especially for the remote communities. The proposed hybrid system uses hydrogen storage system, which is particularly noteworthy for remote area locations that are not connected to electrical grid. In addition, the system is investigated for a case study with a good potential of solar energy and geothermal.

2. Material and methods

2.1. The hybrid geothermal/absorption system

Fig. 1 illustrates the hybrid geothermal/ARS integrated with solar thermal collector, desalination unit and hydrogen storage system. It composes a single flash geothermal system combined with a single effect lithium bromide-water ARS (including production well, reinjection well, flash tank, generator, turbine, heat exchanger (HX), pump, absorber, condenser, evaporator, cooling tower, generator and valve), solar thermal collector, multi-stage flash water desalination system, and hydrogen storage system (comprising electrolyzer, fuel cell, hydrogen storage tank and converter). The geothermal fluid absorbs heat from the production well and goes into the separator. In the separator, the superheated vapor is segregated and goes to the solar collector. Solar energy increases the enthalpy of the geothermal fluid before entering the turbine. The vapor is expanded in the turbine and moved to the condenser. Here, ARS contributes to cooling process. On the plus side, the schemed desalination unit uses the waste energy existing in the refrigerant condenser. It is expected that the process (17 to 18) helps to improve the efficiency of the ARS. Although GE system is a continuous source of energy, combining it with solar energy makes an intermittent production system. Hydrogen production system is proposed to solve the intermittency of the system. The produced hydrogen is applied to generate a stable electrical power by fuel cell. While the generated electricity by the system is higher than the island's requirement, the surplus electricity is dispatched into the electrolyzer. The electrolyzer uses the excess electricity to split water into O_2 and H_2. The generated hydrogen will be transferred into hydrogen tanks. When the produced power is less than the island's need, the fuel cell consumes the stored hydrogen to supply the deficit.

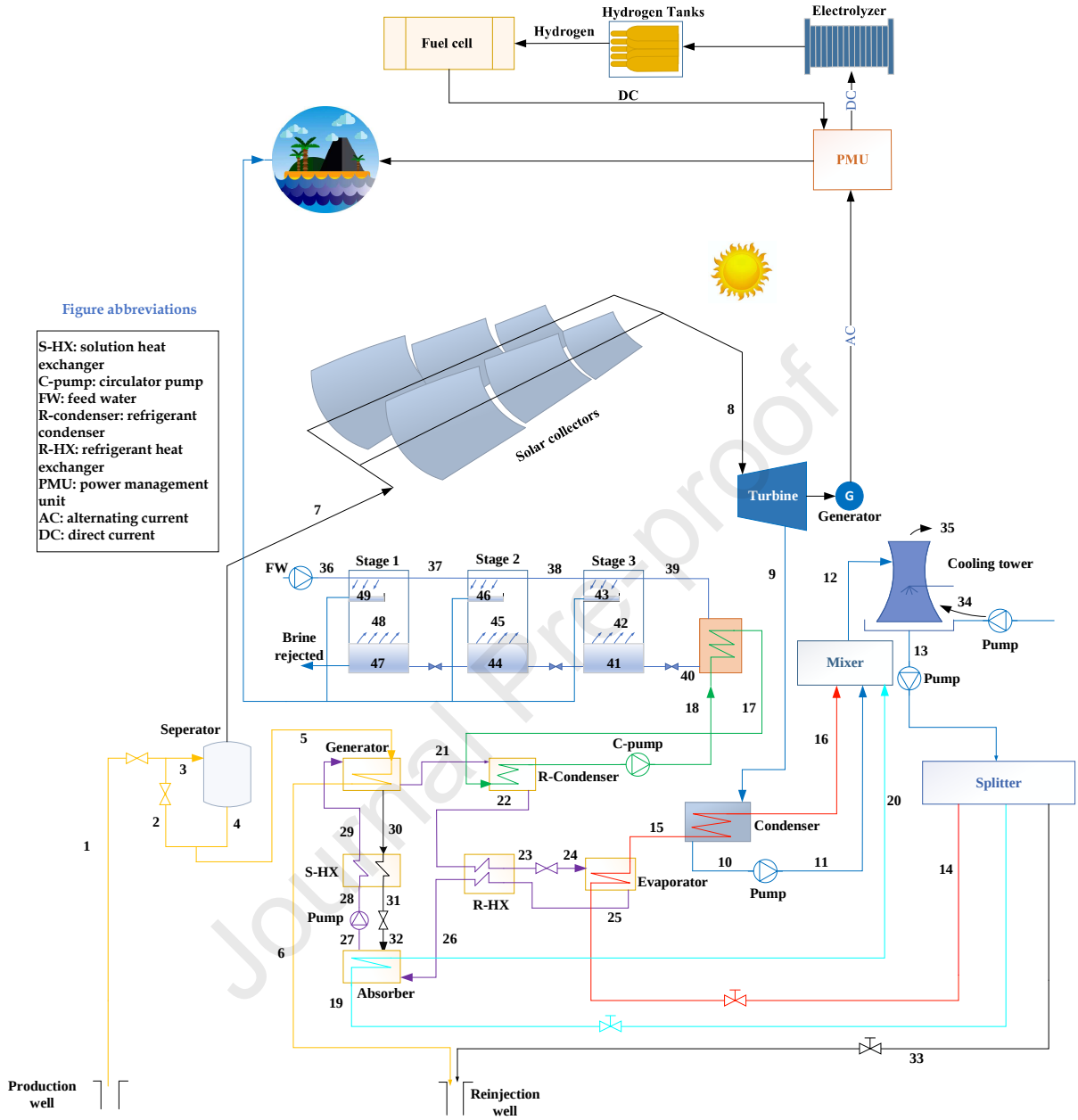

Fig. 1. The hybrid Geothermal/ARS equipped with solar system, desalination unit and hydrogen storage system.

2.2. Mathematical modeling of the hybrid system

2.2.1. Hydrogen storage system

Energy balance for the electrolyzer and fuel cell are:

$$Power\ input = \frac{1}{\eta_{ele}} \dot{m}_{H_2} LHV_{H_2} \tag{1}$$

$$Power\ output = \eta_{FC} \dot{m}_{H_2} LHV_{H_2} \tag{2}$$

2.2.2. Geothermal/ARS

Aqueous lithium bromide solubility is assumed based on mathematical model developed by [28]. The respective thermodynamic relations for each component are as follows.

Solar system

The governing energy equation for solar collector is:

$$\dot{m}_7 h_7 + \dot{Q}_{in,sol} = \dot{m}_7 h_8 \quad (3)$$

Here, P_7 is 950 kPa and the quality of vapor is considered to be 1. Also, $\dot{m}_7$ is calculated by the energy balance for the separator, which is:

$$x_3 = (h_3 - h_4)/(h_7 - h_4) \quad (4.a)$$

$$\dot{m}_7 = x_3 \dot{m}_3 \quad (4.b)$$

$$\dot{m}_4 = (1 - x_3)\dot{m}_3 \quad (4.c)$$

Turbine

Energy balance for the turbine is:

$$\dot{W}_t = \eta_g \dot{m}_7 (h_8 - h_9) \quad (5)$$

Condenser

The corresponding energy equation for the condenser in Rankine cycle (after the turbine) is:

$$\dot{Q}_{cond} = \dot{m}_9 (h_9 - h_{10}) \quad (6)$$

where $T_{cond} = T_{15} + \Delta T_{cond}$ in which ΔT_{cond} is 20℃. Also, P_{cond} is calculated by two independent thermodynamic properties, which are T_{cond} and x=1.

Cooling tower

The governing energy equation for cooling tower is:

$$\dot{m}_{12} h_{12} + \dot{m}_{34} h_{34} = \dot{m}_{13} h_{13} + \dot{m}_{34} h_{35} \quad (7)$$

where thermodynamic properties for point 12 is determined by employing the energy equation for the mixer, which is:

$$\dot{m}_{16} h_{16} + \dot{m}_{11} h_{11} + \dot{m}_{20} h_{20} = \dot{m}_{12} h_{12} \quad (8)$$

Absorber

The energy balance for the absorber in which the refrigerant and absorbent are mixed, is written as:

$$\dot{m}_{32} h_{32} + \dot{m}_{26} h_{26} - \dot{m}_{27} h_{27} = \dot{m}_{19} (h_{20} - h_{19}) \quad (9)$$

where mass conservation law between the refrigerant and the absorbent is defined as a function of the concentration of lithium bromide:

$$\dot{m}_{27} x_{27} = \dot{m}_{32} x_{32} + \dot{m}_{26} x_{26} \quad (10)$$

Also, for a pure refrigerant (without lithium bromide fraction in the refrigerant), the equation is simplified as [16]:

$$\dot{m}_{32} x_{32} = \dot{m}_{27} x_{27} \quad (11)$$

The logarithmic mean temperature difference (LMTD) is employed to ascertain the temperature driving force for heat transfer in the absorber, which is calculated by:

$$LMTD_a = \frac{(T_{32} - T_{20}) + (T_{27} - T_{19})}{ln\left(\frac{T_{32} - T_{20}}{T_{27} - T_{19}}\right)} \quad (12)$$

Solution pump

The energy balance for the pump is calculated by:

$$\dot{m}_{27} h_{27} + \dot{w}_{pump,libr} = \dot{m}_{28} h_{28} \quad (13)$$

$$\dot{w}_{pump,libr} = \frac{\dot{m}_{27}\, v_{27}(P_{28} - P_{27})}{\eta_{pump}} \quad (14)$$

where v_{27}, P and η_{pump} are specific volume, pressure and pump efficiency, respectively.

Solution heat exchanger

After energy balance for the solution heat exchanger (S-HX), the outlet temperature is determined by:

$$T_{31} = T_{28}\eta_{S.HX} + (1 - \eta_{S.HX})T_{30} \quad (15)$$

The LMTD for the S-HX is obtained by Eq. (18):

$$LMTD_{S.HX} = \frac{(T_{30} - T_{29}) + (T_{31} - T_{28})}{ln\left(\frac{T_{30} - T_{29}}{T_{31} - T_{28}}\right)} \quad (16)$$

Generator

Across the desorption process, the fraction of each fluid stream regulates the mass flow equilibrium, which is:

$$\dot{m}_{30} x_{30} = \dot{m}_5 x_5 + \dot{m}_{29} x_{29} \quad (17)$$

The energy balance for the generator is:

$$\dot{m}_{30} h_{30} + \dot{m}_{21} h_{21} - \dot{m}_{29} h_{29} = \dot{m}_5 (h_5 - h_6) \quad (18)$$

and the LMTD for the generator is:

$$LMTD_g = \frac{(T_5 - T_{30}) + (T_6 - T_{29})}{ln\left(\frac{T_5 - T_{30}}{T_6 - T_{29}}\right)} \quad (19)$$

Condenser in ARS

The high-pressure refrigerant vapor is condensed by rejection the vapor's latent heat to the desalination unit, which is calculated by the heat balance for the condenser:

$$\dot{m}_{21}(h_{21} - h_{22}) = \dot{m}_{17}(h_{17} - h_{18}) \quad (20)$$

Moreover, the log mean temperature difference is computed by:

$$LMTD_{cond} = \frac{(T_{21} - T_{18}) + (T_{22} - T_{17})}{ln\left(\frac{T_{21} - T_{18}}{T_{22} - T_{17}}\right)} \quad (21)$$

Evaporator

The lower pressure level of the absorption system is regulated through the evaporation temperature. During evaporation, the two-phase refrigerant is converted into vapor. Energy balance and LMTD for the evaporator are presented by Eqs. (22) and (23).

$$\dot{m}_{14}(h_{15} - h_{14}) = \dot{m}_{24}(h_{24} - h_{25}) \quad (22)$$

$$LMTD_{eva} = \frac{(T_{15} - T_{24}) + (T_{14} - T_{25})}{ln\left(\frac{T_{15} - T_{24}}{T_{14} - T_{25}}\right)} \quad (23)$$

Refrigerant heat exchanger

A refrigerant HX has been considered to improve the overall refrigeration performance in which the heat transfer between the condensed fluid coming from condenser and evaporated fluid coming from evaporator occurs. The efficiency of the refrigeration HX is calculated by:

$$\eta_{R.HX} = \frac{T_{22} - T_{23}}{T_{22} - T_{25}} \quad (24)$$

The relevant energy balance and log mean temperature difference are respectively:

$$\dot{m}_{22}(h_{22} - h_{23}) = \dot{m}_{25}(h_{26} - h_{25}) \quad (25)$$

$$LMTD_{R.HX} = \frac{(T_{22} - T_{26}) + (T_{23} - T_{25})}{ln\left(\frac{T_{22} - T_{26}}{T_{23} - T_{25}}\right)} \quad (26)$$

Energy efficiency of the refrigeration system

For the ARS, the coefficient of performance is defined as:

$$COP_{refrigeration} = \frac{\dot{Q}_{evaporator} + \dot{Q}_{desalination}}{\dot{Q}_{generator} + \dot{W}_{pumps}} \quad (27)$$

The thermal efficiency of the system is presented by:

$$\eta_{cycle,thermal} = \frac{\dot{W}_{net}}{\dot{Q}_{in}} \quad (28)$$

in which $\dot{Q}_{in}$ is the total input energy to the system from geothermal system and solar collector, and the net power output of the cycle is calculated by:

$$\dot{W}_{net} = \dot{W}_t - \dot{W}_{pumps} \quad (29)$$

2.2.3. Desalination unit

As above described in Fig. 1, the required energy for desalination unit is provided by the condenser considered in ARS (process 17 to 18). To analyze the desalination unit, the working fluid is considered as a combination of fluid-solid (water-salt) in which the governing thermodynamic equations for the mixture are considered. The chemical equation for the water-salt mixture is:

$$2NaCl + 2H_2O \rightarrow 2NaOH + H_2 + Cl_2 \quad (30)$$

The salt molar fraction in mixture is presented by:

$$X_{mol,36} = \frac{\frac{x_{36}}{MW_{NaCl}}}{\frac{x_{36}}{MW_{NaCl}} + \frac{1 - x_{36}}{MW_w}} \quad (31)$$

The enthalpy of mixture is calculated by (for point 36):

$$h_{36} = (1 - x_{36}).h(Steam_{IAPWS}, T = T_{36}, x = 0) + x_{36}.cp_{NaCl}.(T_{36} - 273.15\ [K]) \quad (32)$$

In addition, the vapor pressure with a solute is obtained by the following equation:

$$P_{v,1} = \left(1 - 2.X_{mol,36}\right).P_{sat}(Steam_{IAPWS}, T = T_{36}) \quad (33)$$

For stage 1 of the desalination unit, the governing equations are:

$$\dot{m}_{37} = \dot{m}_{36} \quad (34.a)$$

$$x_{37} = x_{36} \quad (34.b)$$

$$X_{mol,37} = X_{mol,36} \quad (34.c)$$

$$P_{37} = P_{36} \quad (34.d)$$

$$Q_{stage\ 1} = m_{37}(h_{37} - h_{36}) \quad (34.e)$$

$$h_2 = (1 - x_{37}).h(Steam_{IAPWS}, T = T_{37}, x = 0) + x_{37}.cp_{NaCl}.(T_{37} - 273.15\ [K]) \quad (34.f)$$

$$P_{v,37} = \left(1 - 2.X_{mol,37}\right).P_{sat}(Steam_{IAPWS}, T = T_{37}) \quad (34.g)$$

The same equations are implemented for stage 2 and stage 3 of desalination unit. Process 39 to 40 is the main process for the desalination in which the obtained energy from ARS is absorbed by the seawater. Here, the seawater is reached to saturation state by attracting the input heat. Therefore, we have:

$$P_{v,40} = P_{40} \quad (35)$$

$$Q_{in,desalination} = \dot{m}_{39}\ (h_{40} - h_{39}) \quad (36)$$

As can be seen, on the back way that is started from point 40, the mixture is in saturation state that by passing through the expansion valve is transformed into the vapor. For calculating the T_{41}, we have:

$$T_{41} = T_{40} + CAT_{stage} \quad (37)$$

and mass balance for this section is:

$$\dot{m}_{40} = \dot{m}_{41} + \dot{m}_{42} \quad (38)$$

Moreover, the capacity of the desalination is calculated by:

$$\eta = 0.001\left[\frac{Q_{in}}{\frac{\dot{m}_{stage\ 1} + \dot{m}_{stage\ 2} + \dot{m}_{stage\ 3}}{1000\ [kg/m^3]}}\right] \quad (39)$$

and $\dot{m}_{sweet}$ is:

$$\dot{m}_{sweet} = \dot{m}_{stage\ 1} + \dot{m}_{stage\ 2} + \dot{m}_{stage\ 3} \quad (40)$$

Table 1 summarizes the technical specifications of the hybrid system considered in this study.

Table 1. Technical specification of the hybrid system.

Parameter	Value	Parameter	Value
Project lifetime (n)	25 years	Efficiency	95%
Air density (ρ_a)	1.22 (kg/m^3)	Nominal power	400 kW
LHV (H_2)	141764 (kJ/kg)	**Hydrogen tank**	
Ambient temperature	25℃	Lifetime	25 years
Ambient pressure	101.3 kPa	Capacity	7000 kg
Geothermal System		Efficiency	95-100%
Well temperature	190℃	**Electrolyzer**	
Well pressure	1255 kPa	Nominal electrolyzer power	350 kW
$\dot{m}_{geo}$	10 kg/s	Electrolyzer efficiency	74%
η_{pump}	0.95	**Fuel cell**	
η_{shx}	0.6	Nominal fuel cell power	800 kW
$T_{pinch,R.HX}$	4℃	Lifetime	10 years
$T_{cooling\ water}$	25℃	**Desalination unit**	

$T_{crystallization\ margin}$	min 10℃	$\dot{m}_{FW}$	10 kg/s
$\eta_{turbine}$	0.85	P_{FW}	150 kPa
$\eta_{generator}$	0.85	T_{FW}	25 ℃
Solar system		$CAT_{stage} = T_{FW} - T_{sat}$	4 ℃
A_{sc}	300 m²	salt fraction	0.035
Lifetime	25 years	MW_{NaCl}	58.44 kJ/kmol
Converter		cp_{NaCl}	630 J/kg-K
Lifetime	10 years		

2.2.4. Economic analysis

The life cycle cost (LCC) is presented by:

$$LCC = CC + MC + IC + RC \tag{41}$$

the economic analysis of the system is carried out based on Eq. (43) in which the annual capital cost (CC), annual maintenance cost (MC), cost of installation (IC) and cost of the replacement of the components is taken into account. Therefore, these parameters are calculated for fuel cell, electrolyzer, hydrogen storage system, converter, geothermal/ARS accompanied by solar collectors and desalination unit, separately. Equation (42) expresses the CC of the fuel cell:

$$CC_{FC} = PW_{FC}\left(\frac{i_r(1+i_r)^{n_p}}{(1+i_r)^{n_p-1}}\right) \tag{42}$$

$$PW_{FC} = C_{FC}\sum_{k=0,10,20}\frac{1}{(1+i_r)^k} \tag{43}$$

in which PW_{FC} is the single payment present worth factor and C_{FC} is the fuel cell cost. The same equation can be applied for the CC calculation of electrolyzer. Likewise, capital cost of the hybrid geothermal/ARS is calculated by:

$$CC_{Geo/Abs} = C_{Geo/ARS}\left(\frac{i_r(1+i_r)^{n_p}}{(1+i_r)^{n_p-1}}\right) \tag{44}$$

where $C_{Geo/ARS}$ is the fixed capital investment of the system. The economic analysis is carried out based on the considered assumptions proposed by National Renewable Energy Laboratory (NREL) [29]. For geothermal system, drilling and associated costs (including exploration and confirmation; production and injection; surface equipment, installation and stimulation cost; over-riding calculated costs), plant capital cost, pump cost inputs, and recapitalization cost are considered. Here, total direct cost is obtained as 3335.4 $/kW and total installed cost per capacity is 4622 $/kW. Moreover, indirect capital cost is considered as: engineer, procure, construct=12% of direct cost; project, land, Miscellaneous=3.5% of direct cost; sales tax of 5% applies to 80% of direct cost. More details are summarized in Table 2.

Table 2. The considered economic parameters for the hybrid system.

Parameter	Value	Parameter	Value
Geothermal/absorption system		**Hydrogen tank**	
Total direct cost	3,335 $/kW	Initial cost	500 ($/kg)
Indirect capital cost: engineer, procure, construct project, land, Miscellaneous sales tax	12% of direct cost 3.5% of direct cost 4% of direct cost	Annual costs of the maintenance	5% of total cost-year
Total installed cost per capacity	4,622 $/kW	**Electrolyzer**	
Contingency	7% of total	Initial cost	1500 ($/kW)
Annual costs of the maintenance	5% of total cost-year	Number of units	3
Solar field		electrolyzer replacement cost	$1400
Site improvements	25 $/m²	Annual costs of the maintenance	5% of initial cost-year
Solar field	150 $/m²	**Fuel cell**	
Contingency	7% of total	Initial cost	2000 ($/kW)
Annual costs of the maintenance	5% of total cost-year	Number of units	3
Converter		Annual costs of the maintenance	5% of the initial cost
Initial cost	700 ($/kW)	Fuel cell replacement cost	$1400
Number of units	3	**Desalination unit**	$100,000

2.3. Intelligent Methods

Fig. 2 (b) shows a multilayer neural network that is sketched to simulate the behavior of the hybrid geothermal/ARS combined with solar collector. The intelligent methods are employed to fulfill nonlinear statistical modeling and prepare a new substitute for conventional regression methods. The goal of this research is developing an intelligent method to understand the effect of input parameters on the targets. These intelligent methods are implemented to utterly discover intricate nonlinear patterns between inputs and targets (as can be observed in Fig. 2 (a)). The network is manufactured based on solar irradiance, cooling water temperature difference $\left(\Delta T_{cooling} = T_{14} - T_{15}\right)$, pinch-point temperature $\left(T_{pinch,absorber} = T_{27} - T_{19}\right)$, ambient temperature, evaporating temperature and condensing temperature as input variables. The intelligent methods apply the input parameters to estimate the produced power, coefficient of performance ($COP_{chiller}$) of ARS, total heat exchanger area (HXA) of the ARS, and cycle thermal efficiency. For this purpose, MLP neural network optimized ICA, (MLP-ICA), is developed and compared with MLP-GA. The network training is carried out using 70% of data, 30% of dataset are adapted to test the network. Two statistical indicators are employed to appraise the prediction accuracy of the intelligent methods, which are expressed by Eqs. (45) and (46).

$$RMSE = \sqrt{\frac{1}{n}\sum_{i=1}^{n}(x_i - y_i)^2} \tag{45}$$

$$R = \frac{\sum_{i=1}^{n}(x_i - \bar{x})(y_i - \bar{y})}{\sqrt{\sum_{i=1}^{n}(x_i - \bar{x})^2 \sum_{i=1}^{n}(y_i - \bar{y})^2}} \tag{46}$$

where x_i, y_i, $\bar{x}$, $\bar{y}$ and n are real data, predicted data, mean of real data, mean of predicted data and number of data, respectively.

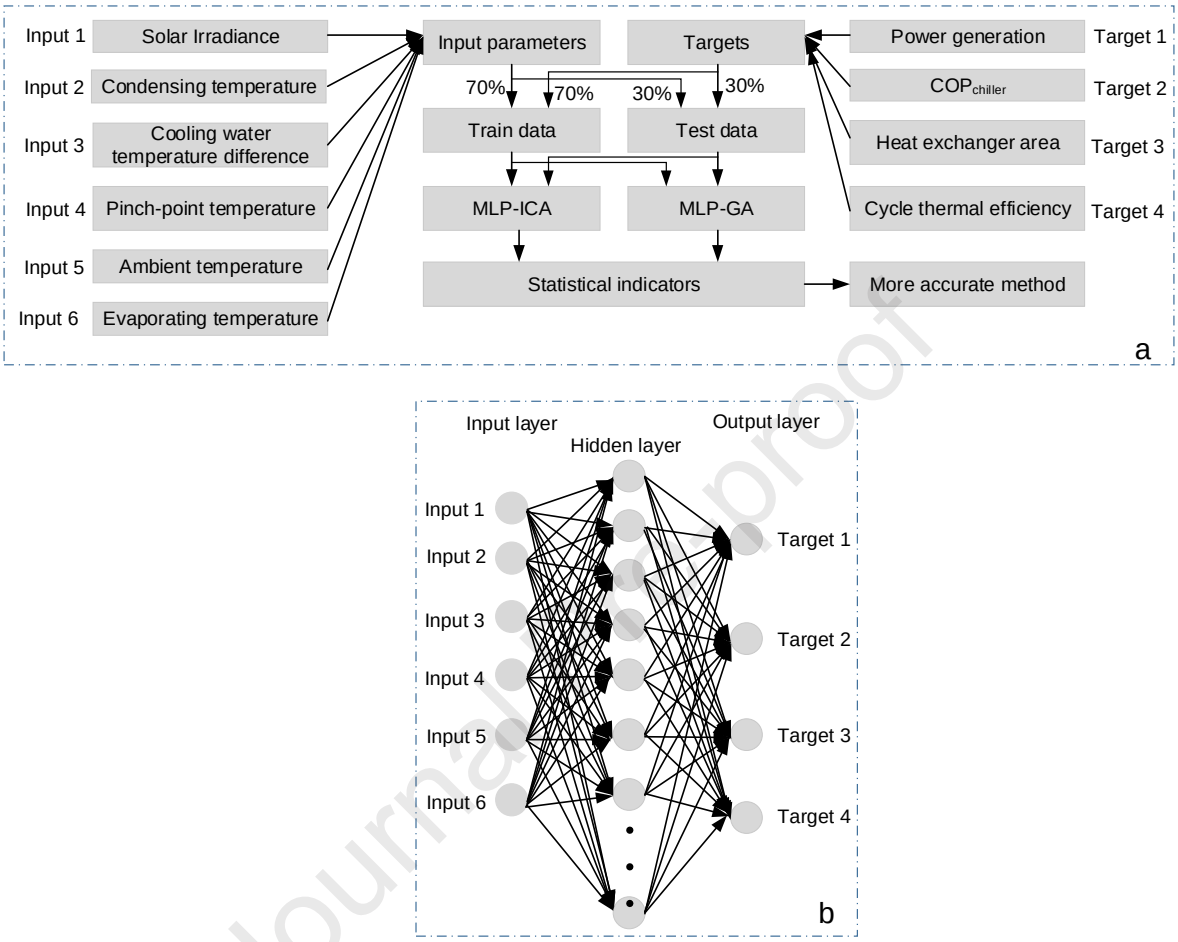

Fig. 2. The proposed structure for modeling the geothermal/ARS (a), a schematic of multilayer neural network (b).

2.3.1. Mathematical Modeling of the Intelligent Methods

The hybrid MLP-ICA and MLP-GA are developed based on seven steps including data loading, normalization, training and testing datasets, network structure, training the network using the corresponding optimization algorithm, assessment and display. In step 5, the network is trained using the respective optimization algorithm (GA for MLP-GA and ICA for MLP-ICA). Indeed, here, the optimum values of input weight matrix, bias vector and layer weight matrix are determined by the external functions that are ICA and GA combined with MLP.

[30] by inspiration of imperialist competition introduced a new evolutionary algorithm called imperialist competitive algorithm (ICA). Similar to other evolutionary algorithms that are adapted for optimization problems, ICA also initiates with a primary population. Population individuals are defined as country, which are recognized in two species: colonies and imperialists that as a group establish some empires. The foundation of ICA is formed using imperialist competition between the empires. The feeble empires within this competition crumble and strong ones grab possessions of their colonies. In the following, the imperialist competition converges to a situation where

only one empire and its colonies are in the same state and possess the similar cost as imperialist. Fig. 3 represents ICA algorithm in eleven steps.

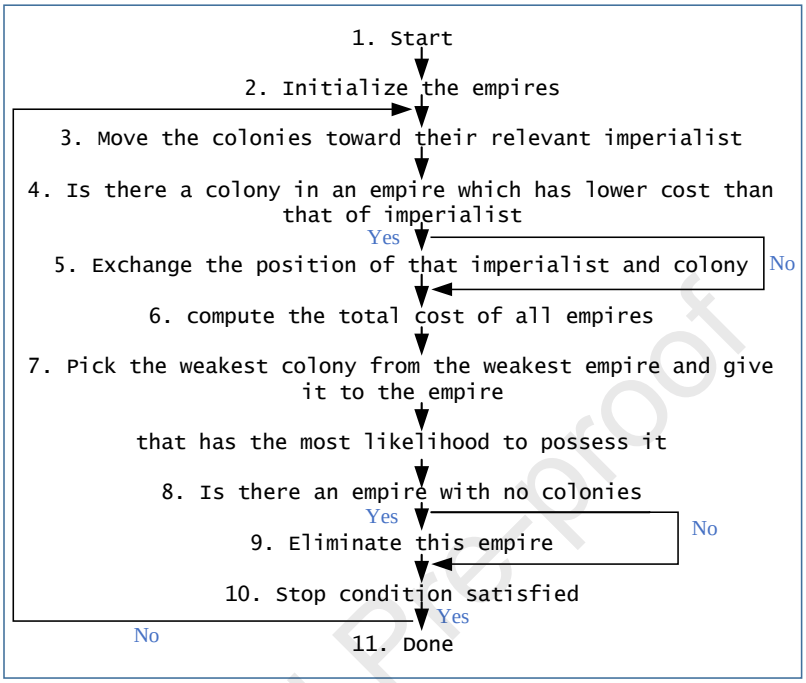

Fig. 3. Structure of imperialist competitive algorithm.

3. Case study

In the current research, case study is Sirri Island located in the south of Iran in the Persian Gulf. The island is approximately 5.6 kilometers long with a width of around 3 kilometers, with the area of 17.33 square kilometers and population of 1304. Fig. 4 depicts the mean values of solar irradiance for Sirri Island during 2018 [31]. This figure shows that in the most of time the average solar irradiance on a horizontal collector is higher than 5 ($kWh/m^2.day$). Since 1975, extensive studies have been carried out to figure out the potential of GE across the country by the Ministry of Energy [32]. The result of this potentiometric analysis was shown that $1.087 \times 10^{19}\ kJ$ of GE can be extracted by geothermal technology. During the project entitled "The Geothermal Potential Survey in Iran", ten regions with a significant amount of GE in which the studied area in this research was one of them, were identified and introduced [33].

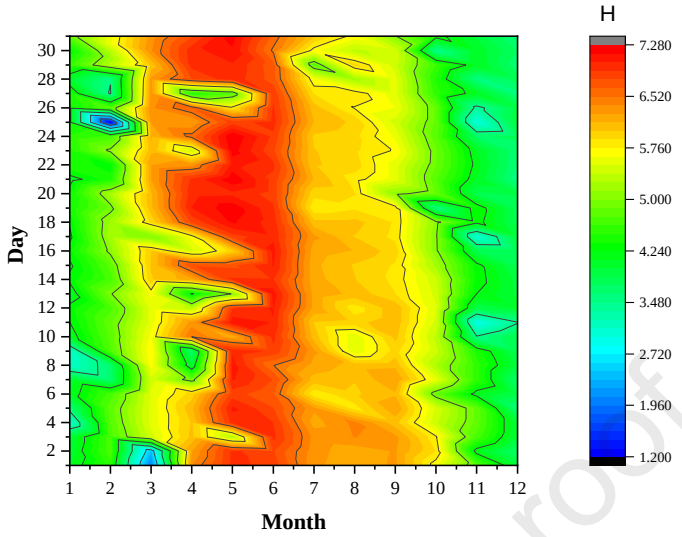

Fig. 4. Solar radiation on a horizontal collector at Sirri island, Iran in 2018 (kWh/m².day).

4. Results and Discussion

In this research, a hybrid geothermal/ARS equipped with solar collector, desalination unit and hydrogen storage system was developed and appraised by implementing a thermodynamic model and two intelligent methods. The influence of the momentous design criterions of the hybrid system (comprising solar irradiance, condensing temperature, cooling water temperature difference, pinch-point temperature, ambient temperature and evaporating temperature) upon power generation, $COP_{chiller}$, total HXA of the ARS, and cycle thermal efficiency were assessed. A simple configuration of geothermal/ARS as well as its thermodynamic model was developed by [34] and [35]. To validate the results of thermodynamic model a simple geothermal/ARS was implemented. For evaporation temperature of 8.5 ℃, absorber temperature of 30 ℃ and generator temperature of 60 ℃, the COP of refrigeration system for this study was obtained 0.7428. This COP was reported around 0.7591 in [34] in which the error is around 2.41%. The results of this research are presented in the following.

4.1. Power generation

Figure 5 (b) shows the electrical power demand for the island in a period of one year. It is apparently seen that the power demand for the island from April to September is more than 900 kW. Figure 5 (a) depicts the power generation by the hybrid system for the entire year (more specifically, produced power by the system for January and June is presented in Fig. 5 (c)). It could be plainly viewed that the generated power by the system from April to September is more than the other months. Comparison between Fig. 5 (a) and Fig. 5 (b) shows that although the peak point for the power demand is more than the power generation, applying the hydrogen storage system can circumvent this problem.

Figure 6 (a) displays the surplus power dispatched into the electrolyzer throughout the year. The electrolyzer uses this surplus power for producing the hydrogen so long as the generated power by the system is more than the island's requirement. Due to having the high demand from April to September, the excess power transferred to the

electrolyzer is less than the other months. Whenever the power demand of the island is lower than the generated power by the system, the fuel cell provides the deficit. Figure 6 (b) represents the generated power by the fuel cell for the entire year in the study region.

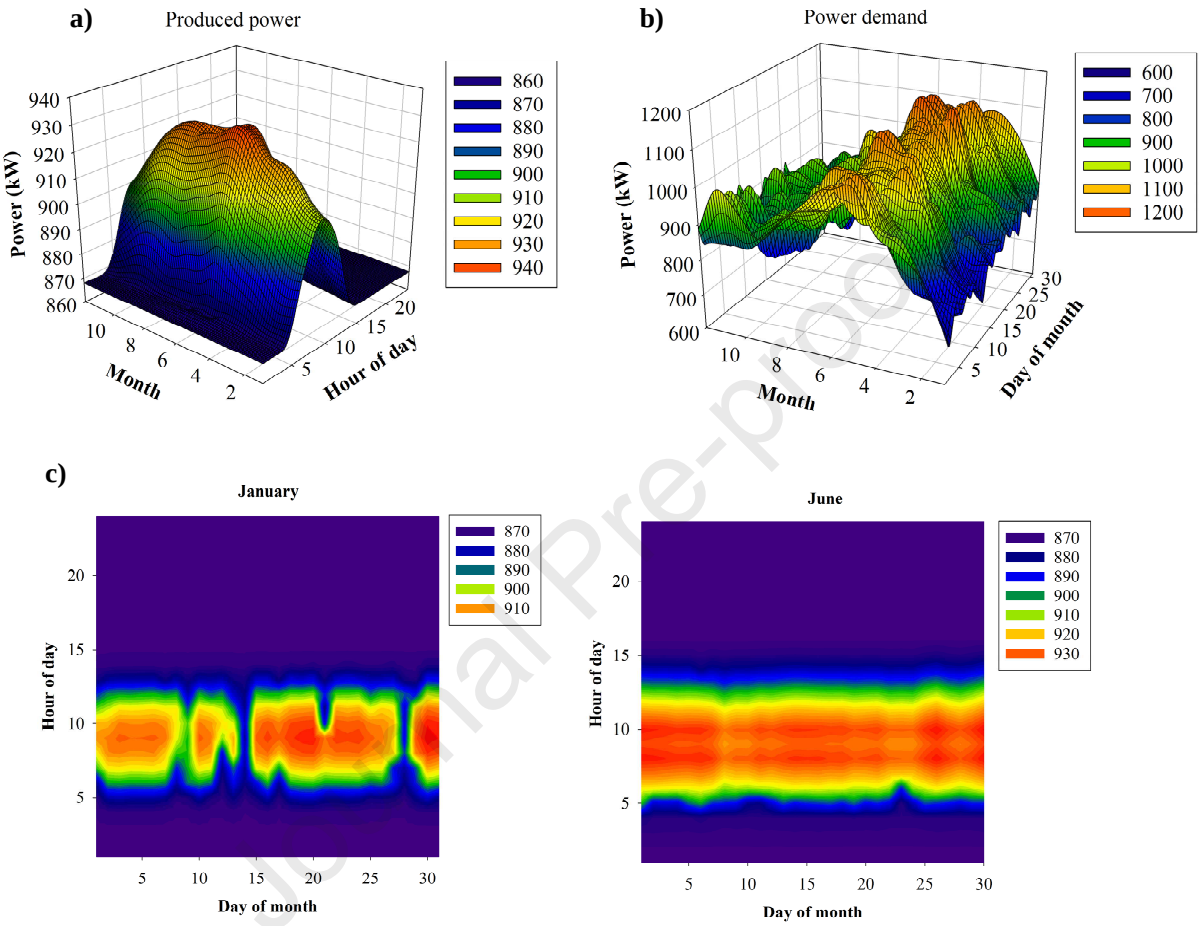

Fig. 5. Power generation by the system during one year (a), the pattern of power demand of the island (b), produced power by the system in January and June (c).

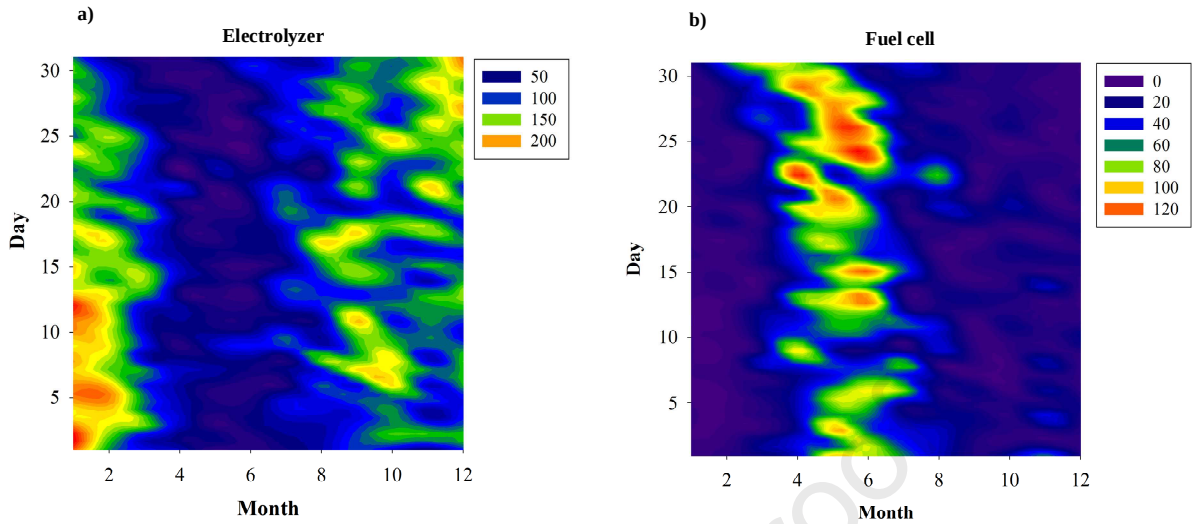

Fig. 6. The excess power (kW) transferred to the electrolyzer (a) and generated power by the fuel cell (b) during a period of one year.

Figure 7 demonstrates the storage pattern of the hydrogen for entire year in the case study region. It can be observed that between January and March the trend is increasing, afterward, from March to September the stored hydrogen by the system is used by the fuel cell to meet the power demand of the island. From September to December, the hybrid system can store the hydrogen and the value of stored hydrogen in the storage system will be increased.

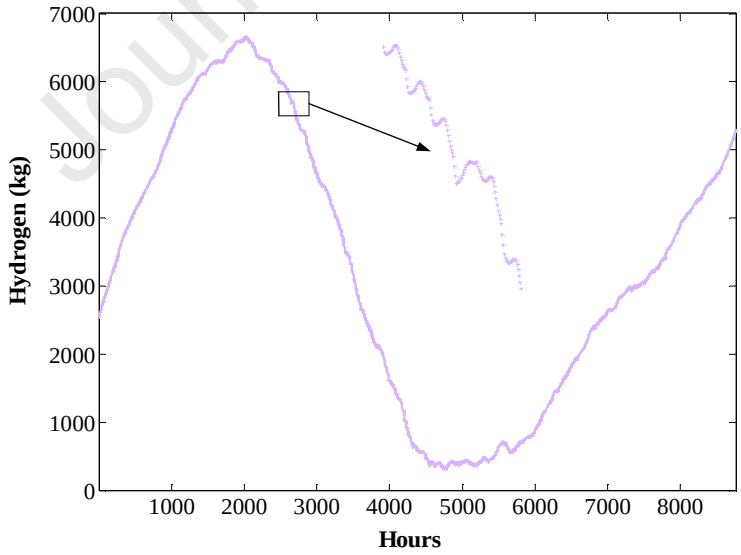

Fig. 7. Storage pattern of hydrogen throughout the year.

Figure 8 illustrates the train and test phases of the MLP-ICA to estimate the power produced by the hybrid system. As mentioned above, two statistical indicators have been employed for assessing the prediction accuracy of

the intelligent methods. For prediction of power generation by MLP-ICA, the statistical metrics were obtained as R_{train}= 0.9965, R_{test}=0.9944, $RMSE_{train}$=1.5812 (kW) and $RMSE_{test}$=2.2390 (kW) (the values of MSE presented in Fig. 8 are $RMSE^2$). A can be seen in Fig. 8, the MLP-ICA can meticulously estimate the power generation using the input parameters.

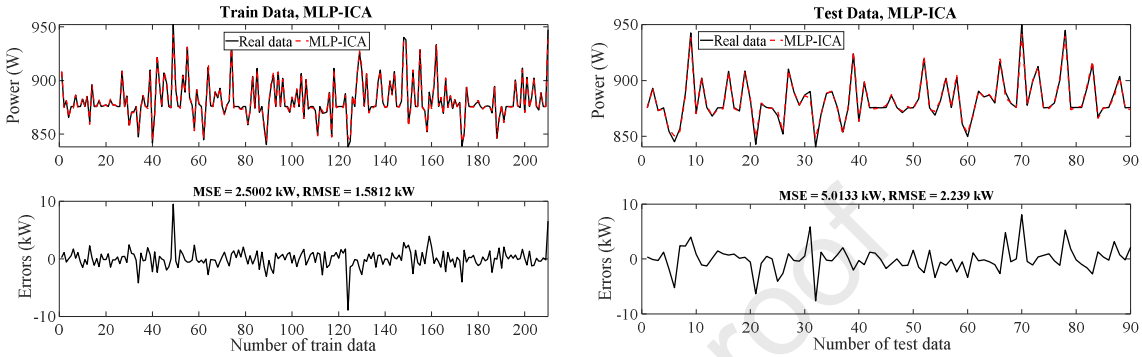

Fig. 8. Training and testing stage of MLP-ICA for predicting the cycle net power output.

The power generation also was modeled by the MLP-GA method, which the result of this modeling is shown in Fig. 9 as well. For this prediction, the statistical metrics were obtained as R_{train}= 0.9884, R_{test}=0.9853, $RMSE_{train}$=3.3013 (kW) and $RMSE_{test}$=3.6175 (kW). By comparing the statistical parameters employed for assessing the performance of the MLP-ICA and MLP-GA, it can be concluded that the prediction accuracy of the MLP-ICA is superior to the MLP-GA.

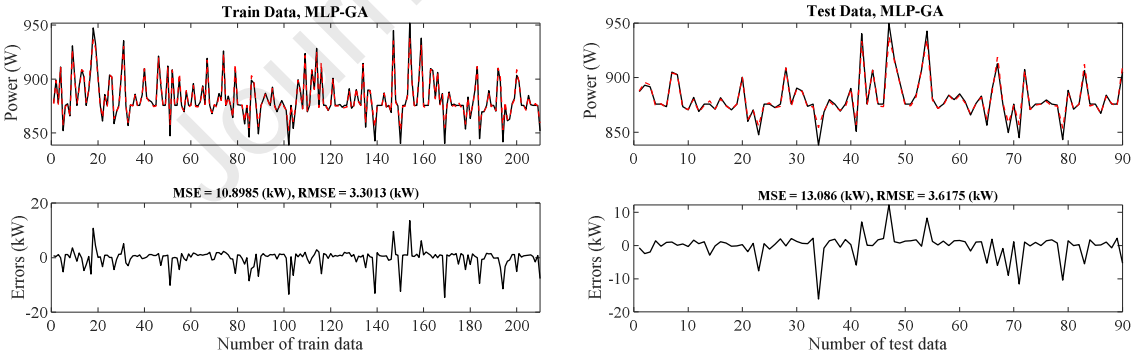

Fig. 9. Training and testing phases of MLP-GA for estimating the cycle net power output.

Figure 10 indicates the influence of the input variables over the power generation of the hybrid system. Fig. 10 (a) represents the variation of the produced power versus the solar irradiance. It is explicitly observed that enhancing solar irradiance enhances the produced power of the system. The reason is described as increasing the inlet enthalpy to the turbine, which the turbine can catch more energy from the working fluid. Fig. 10 (b) illustrates the influence of the cooling water temperature difference ($\Delta T_{cooling} = T_{14} - T_{15}$) on the power generation. It could be plainly viewed that, when $\Delta T_{cooling}$ goes up, the generated power by the system raises as well. The temperature of the

cooling water has an adverse effect upon the condenser pressure resulting in decreasing the work of the turbine. The low temperature cooling water causes condensing the steam in lower pressure environment. The availability of low condenser pressure increases the enthalpy differences between the input and output of the turbine so the net power output raises. Fig. 10 (c) depicts that enhancing the environment temperature declines the power generation of the system. Fig. 10 (d) represents the alteration of the power generation versus the increment of the condensing temperature. Clearly, the power generation has a tendency to decline as the condensing temperature increases. Indeed, the availability of low condensing temperature can cause achieving high performance of power generation. The lower amount of cooling water temperature causes a low pressure of the Rankine cycle component, particularly for the steam condenser. Other input parameters do not influence power generation. Figs. 10 (e) and 10 (f) demonstrate the decision surface for modeling of power generation versus input variables to the network.

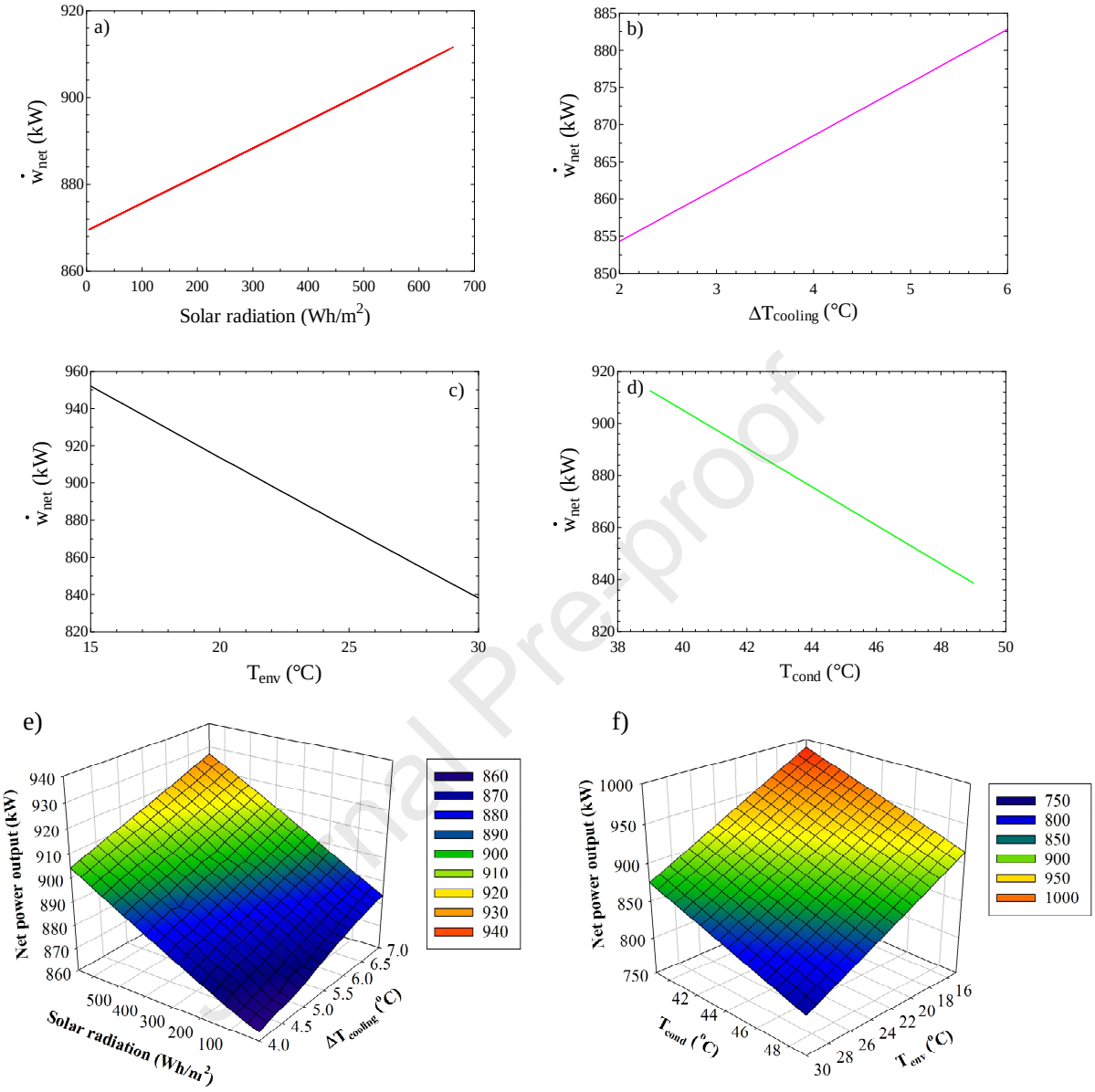

Fig. 10. The result of the input variables on the generated power of the hybrid system; (a) solar radiation; (b) cooling tower temperature difference; (c) environment temperature; (d) condensing temperature; (e) decision surface for (a)and (b); decision surface for (c) and (d).

4.2. $COP_{chiller}$

Fig. 11 represents the testing phases of the MLP-ICA and MLP-GA methods for forecasting the $COP_{chiller}$. For this prediction the statistical parameters have been obtained as R_{train}= 0.9969, R_{test}=0.9982, $RMSE_{train}$=0.0023 and $RMSE_{test}$=0.0014, for the MLP-ICA; and R_{train}= 0.9905, R_{test}=0.9918, $RMSE_{train}$=0.0037 and $RMSE_{test}$=0.0044, for MLP-GA. As can be observed, the MLP-ICA performs better than the MLP-GA for forecasting the $COP_{chiller}$.

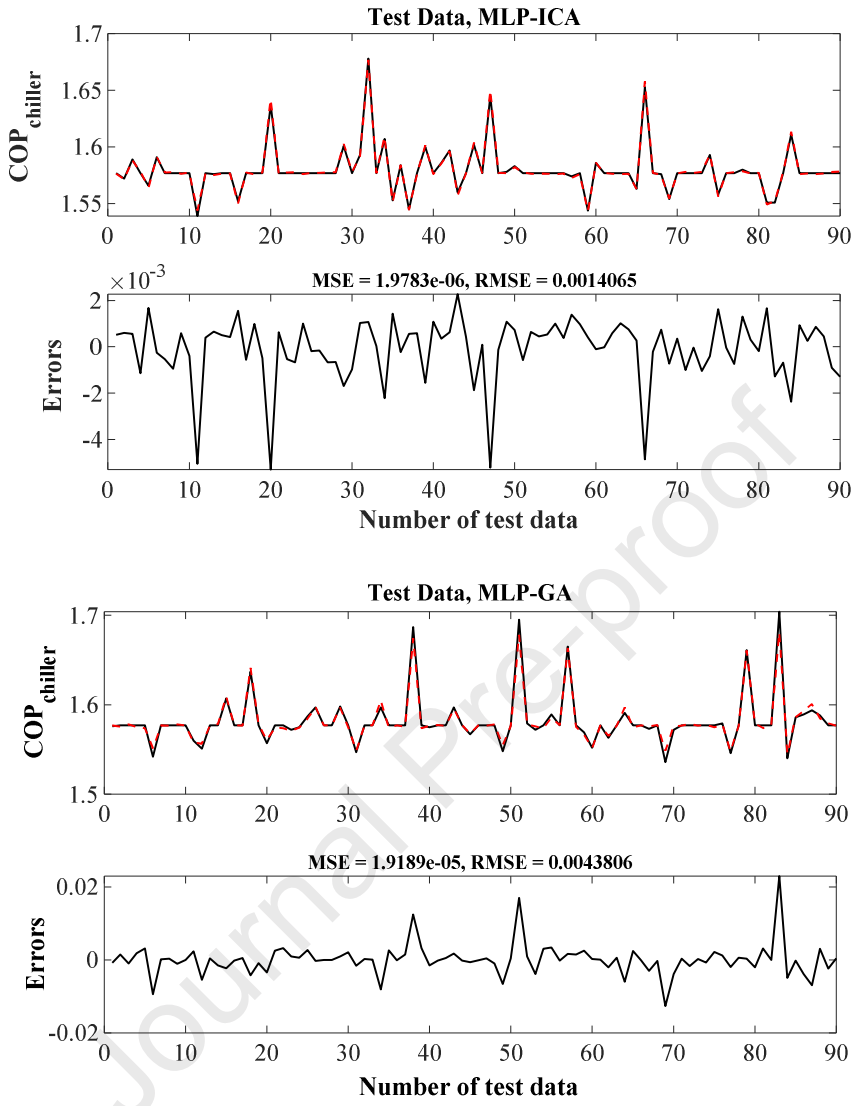

Fig. 11. Test data of the MLP-ICA and MLP-GA for forecasting the $COP_{chiller}$.

Figure 12 (a) depicts the variation of the $COP_{chiller}$ versus the pinch-point temperature $\left(T_{pinch,absorber} = T_{27} - T_{19}\right)$. According to the figure, when the pinch-point temperature increases, the $COP_{chiller}$ declines. At a constant pressure, for the greater values of solution temperature, the absorber requires more absorbent to entirely absorb the same refrigerant value. As a result, when the refrigerant mass flow is constant, higher values of absorbent mass flow is required. By increasing the mass flow, the heat transfer inside the absorber and generator enhances as both are in relation to the same solution mass flow. For this reason, the ARS needs extra heat to work satisfactorily. For the constant refrigeration capacity, extra heat declines the performance of the machine as is presented in Fig. 12 (a). Enhancing the environment temperature decreases the COP of the ARS as is depicted in Fig. 12 (b). The result of evaporation temperature on the COP of the refrigeration system is shown in Fig. 12 (c). As presented in Fig. 12 (c), raising the evaporation temperature, increases the COP of the system. Evaporation temperature is one of the main

variables to control the total heat demand for the refrigeration system. There is no influence of other input parameters over $COP_{chiller}$.

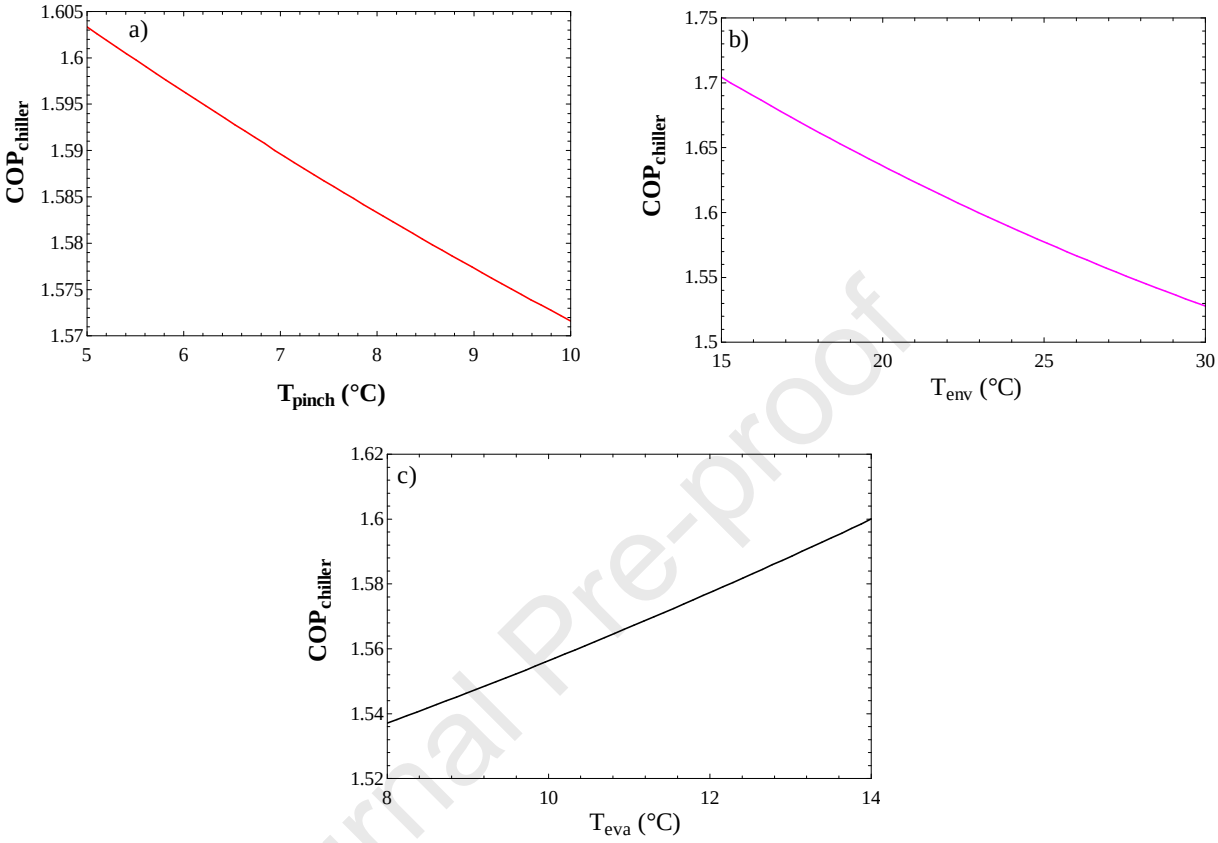

Fig. 12. The variation of $COP_{chiller}$ versus pinch-point temperature (a), environment temperature (b), and evaporating temperature (c).

4.3. Total Heat Exchanger Area

The third target that has been modeled by intelligent methods is the total HXA of the ARS. Fig. 13 shows the test data of the MLP-ICA and MLP-GA for forecasting the A_{HX}. For this prediction, the statistical metrics have been achieved as R_{train}= 0.9933, R_{test}=0.9936, $RMSE_{train}$=4.7362 m^2, and $RMSE_{test}$=4.3069 m^2, for the MLP-ICA; and R_{train}= 0.9786, R_{test}=0.9846, $RMSE_{train}$=9.5831 m^2 and $RMSE_{test}$=8.1047 m^2, for MLP-GA. Performance comparison between the intelligent methods shows that the MLP-ICA works better than the MLP-GA for forecasting the A_{HX}.

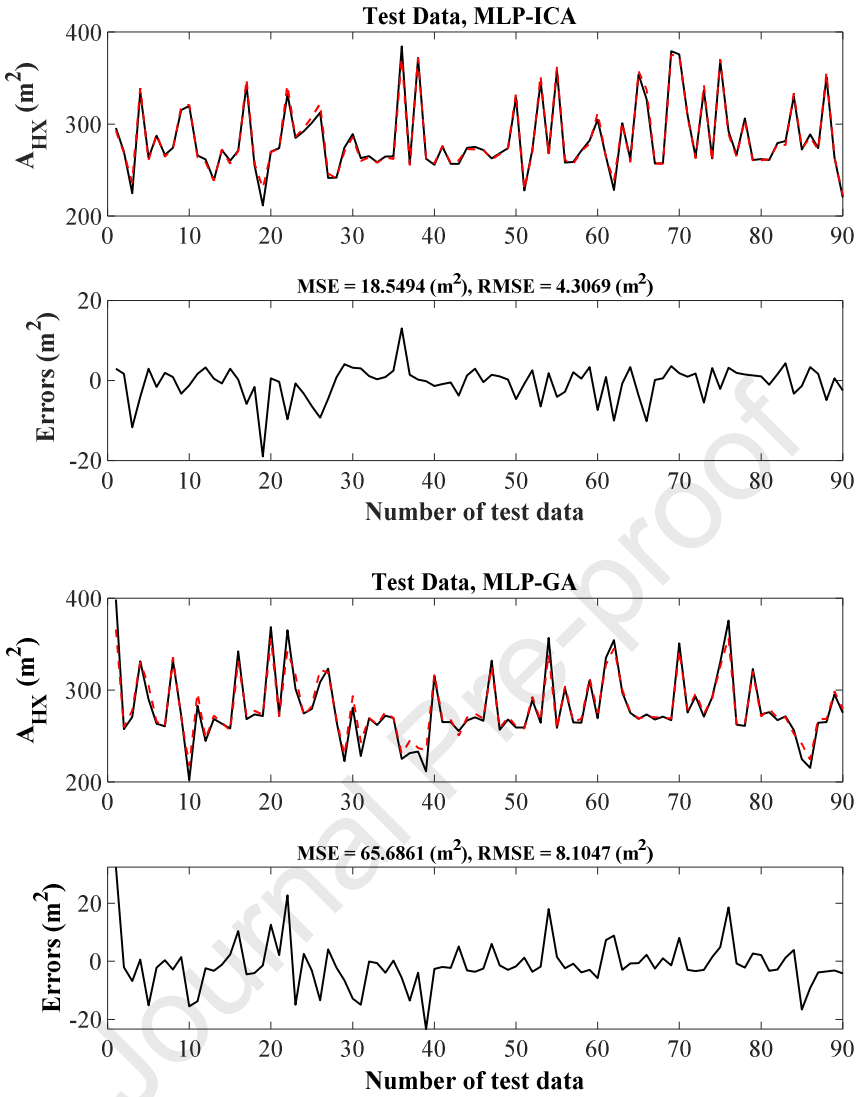

Fig. 13. Test data of the MLP-ICA and MLP-GA for estimating the A_{HX}.

Fig. 14 depicts the variation of the total HXA versus the solar radiation (a), pinch-point temperature (b), cooling water temperature difference (c), environment temperature (d), evaporating temperature (e) and condensing temperature (f). The required HXA for the refrigeration system is specified by the LMDH method since the overall heat transfer coefficient for HXs is constant. Fig. 14 indicates that the total HXA of the system has a tendency to increase as solar radiation, cooling water temperature difference and evaporation temperature enhance, and pinch-point temperature, environment temperature and condensing temperature decrease.

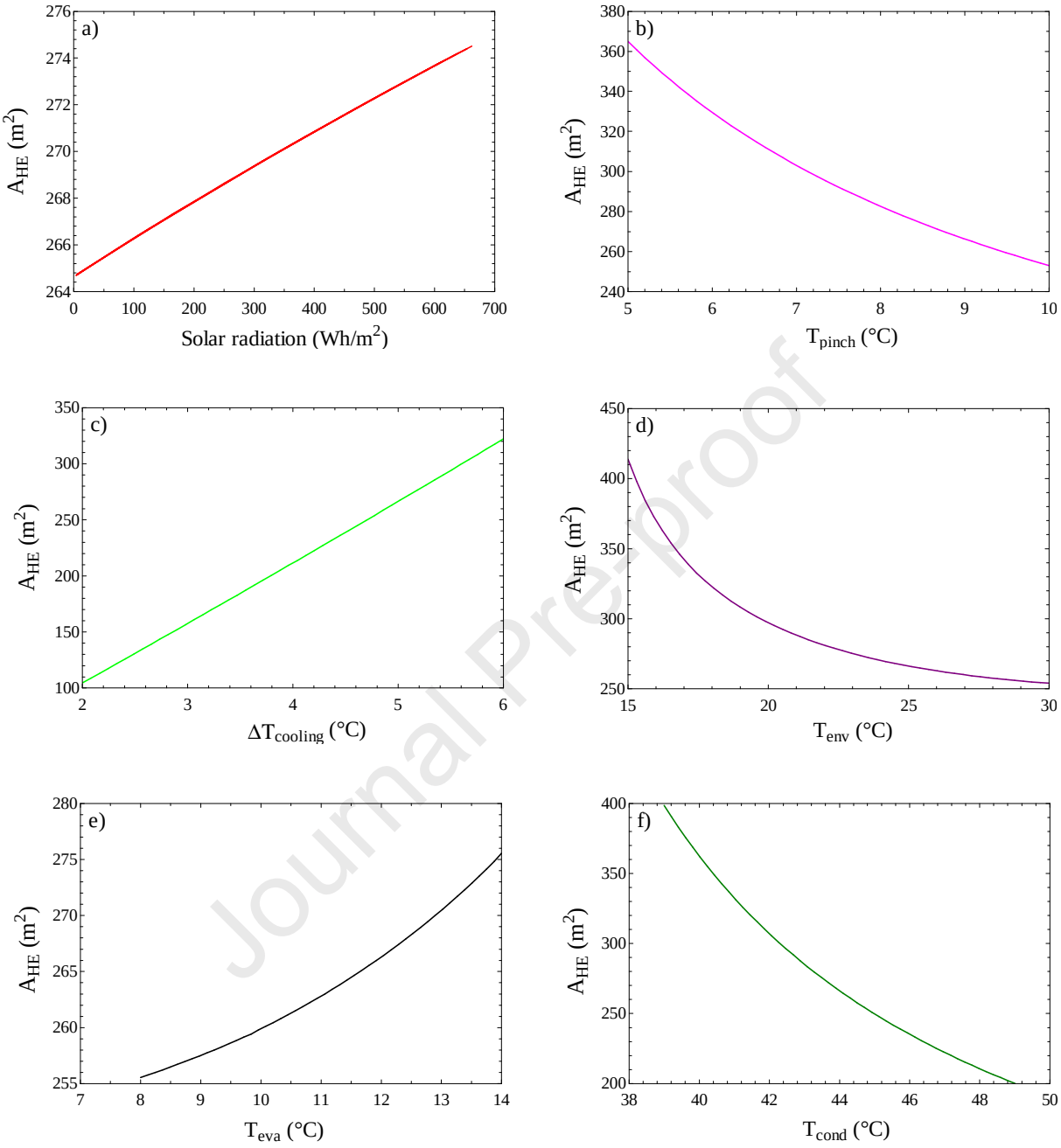

Fig. 14. The influence of solar radiation (a), pinch-point temperature (b), cooling water temperature difference (c), environment temperature (d), evaporating temperature (e) and condensing temperature (f) over the A_{HX}.

4.4. Cycle thermal efficiency

According to Eq. (28), thermal efficiency of the hybrid system was described as a ratio of net energy output to energy input. From input parameters to the network, variation of solar radiation, cooling water temperature difference, condensing temperature, and environment temperature vary the cycle thermal efficiency. This behavior was simulated by intelligent methods and Fig. 15 depicts the testing stage of the MLP-ICA and MLP-GA for modeling the cycle thermal efficiency. The statistical parameters were obtained as R_{train}= 0.9958, R_{test}=0.9955,

$RMSE_{train}$=2.4314e-04 and $RMSE_{test}$=1.9131e-04, for the MLP-ICA; and R_{train}= 0.9918, R_{test}=0.9907, $RMSE_{train}$=3.4028e-04 and $RMSE_{test}$=4.6108e-04, for MLP-GA.

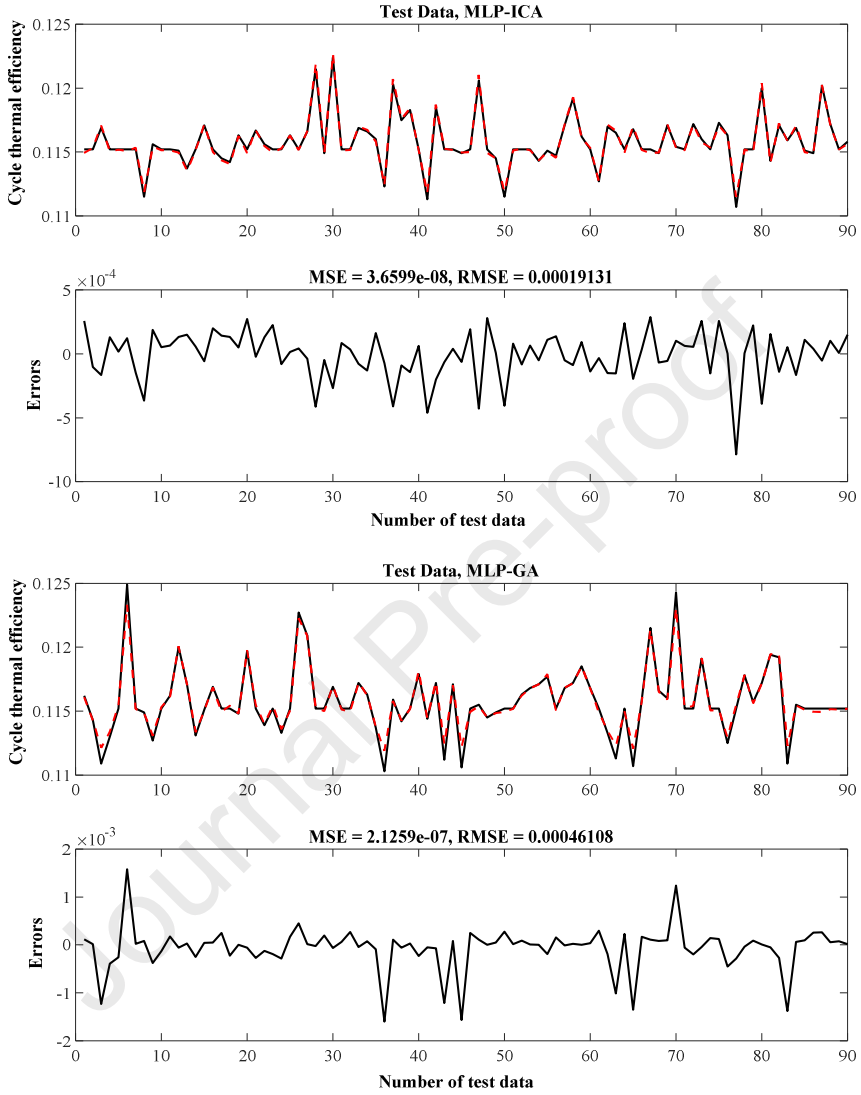

Fig. 15. Testing stage of MLP-ICA and MLP-GA for modeling of the cycle thermal efficiency.

The variation of the cycle thermal efficiency versus the input parameters to the network was presented in Fig. 16. It is clear that increasing the solar irradiance and cooling water temperature difference increases the cycle thermal efficiency (Figs. 16 (a) and 16 (b)). Besides, variation of the cycle thermal efficiency versus environment and condensing temperature is presented in Figs. 16 (c) and 16 (d). The figures show that increasing the environment and condensing temperature decreases the cycle thermal efficiency.

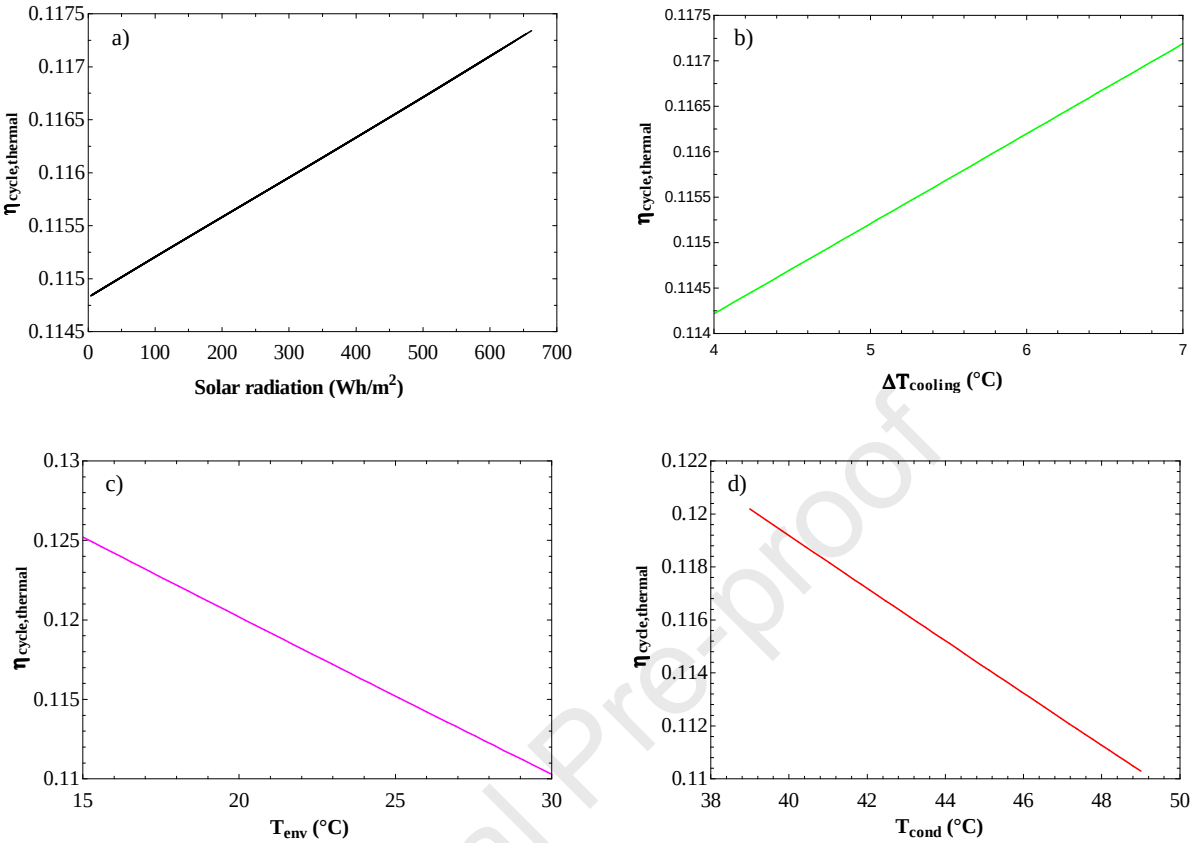

Fig. 16. The variation of the cycle thermal efficiency versus solar radiation (a), cooling water temperature difference (b), environment temperature (c) and condensing temperature (d).

4.5. Desalination unit

According to Fig. 17 (c), the desalination capacity of the unit by considering $Q_{in,desalination} = 900\,kW$, is around 10,000 kJ/m^3 with which the unit can produce 3.2 m^3/h sweet water. This figure reveals that increasing the input energy to the desalination unit, decreases the desalination capacity and increases the produced sweet water. The total sweet water is attained with the sum of condensed water in each stage. Figure 17 (b) illustrates the produced sweet water in each stage in which the stage 3 produces more sweet water as expected. Fig. 17 (a) depicted the transferred energy in each stage in which this value for stage 3 is higher than stages 2 and 1.

Figure 18 (a) represents that by adding the desalination system and using the waste energy of ARS condenser, the $COP_{chiller}$ significantly increases. Fig. 18 (A) shows variation of the COP for the hybrid system by considering the desalination system (SD) and without it (S). For a refrigeration system, COP is described as the ratio of desired output to the required input. Here, the energy input to the system is constant and it comes from geothermal sources and solar thermal collector and only by considering desalination unit the desired output of the system increases resulting in increasing the COP. Besides, a slight increase is seen for the produced power by the hybrid system. It is due to decreasing the total pumping work according to Eq. (29).

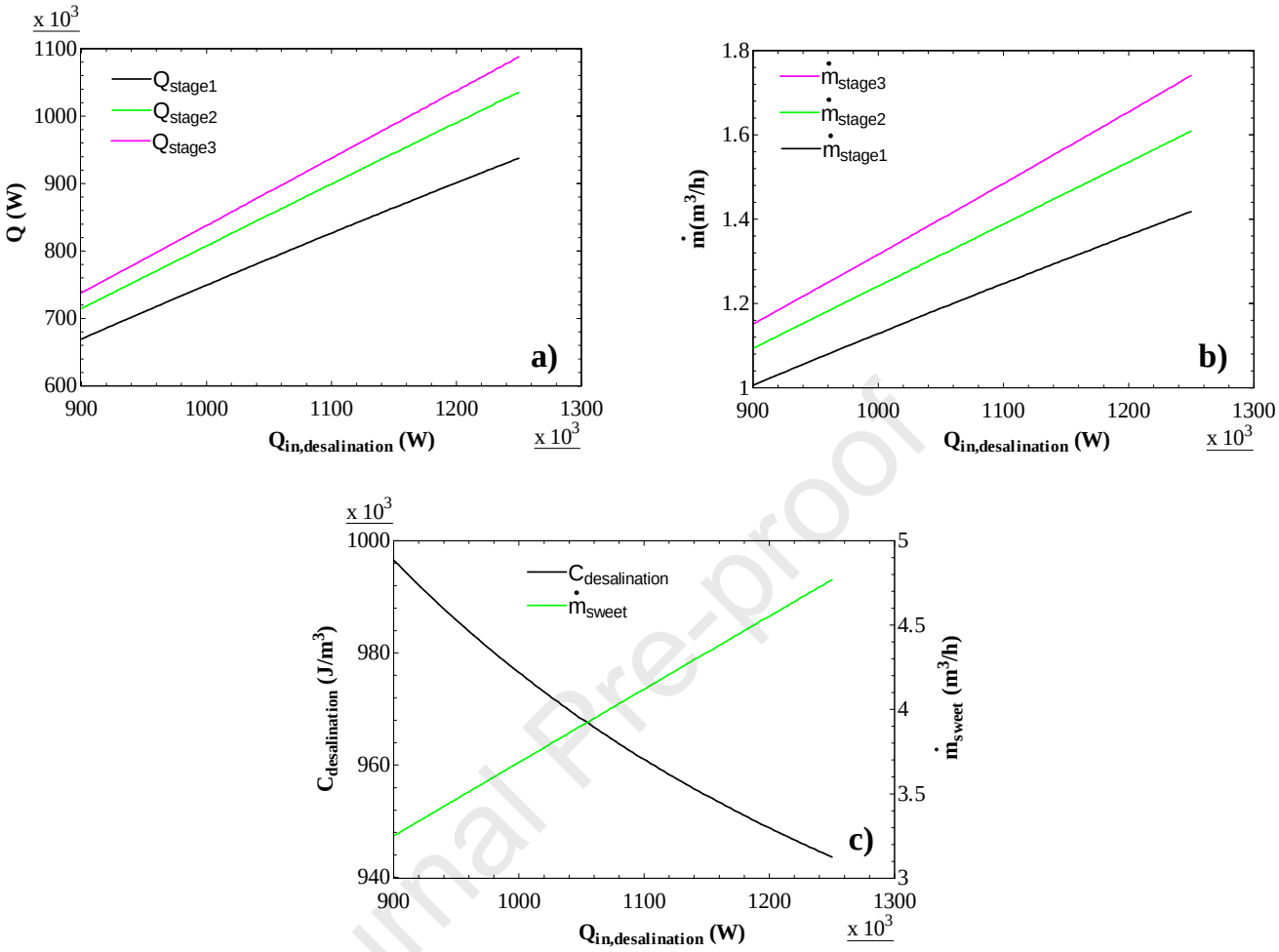

Fig. 17. Desalination unit: heat transfer in each stage (a), produced sweet water in each stage (b), desalination capacity and the total sweet water (c).

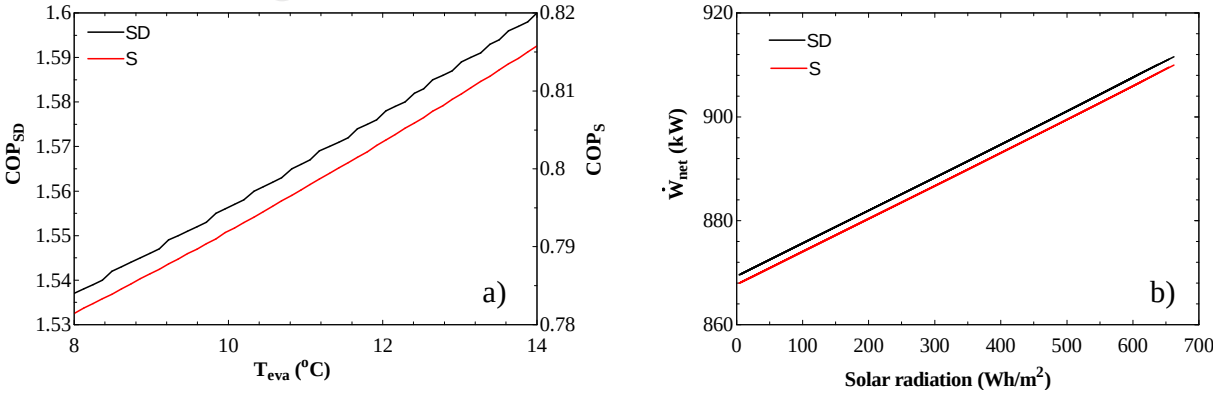

Fig. 18. The COP of the system including desalination (SD) and without desalination (S) (a), and power generation of the system against solar radiation (b).

4.6. Economic Analysis

The economic assessment also was implemented to evaluate the proposed hybrid system in the study region. Figure 19 shows the initial investment of the system's components in which the geothermal system (including GE section, ARS and solar thermal collector) possesses the maximum portion (40%). We can see that the hydrogen tanks boasted an impressive 25% of the total initial investment. Predominantly, for the hydrogen storage system, some challenges have been revealed. Among them, the high initial investment and low efficiency of the storage process have been underscored. Notwithstanding for remoteness regions, to supply the energy demand, the energy transmission costs, grid construction costs and the availability of fuels during the year should be considered as well. Also, energy storage systems can cover the problem of alternating energy produced by RESs. On the plus side, the use of electricity storage system is warranted by the capacity restriction of grids. For instance, in the case of wind farms, the wind turbines are installed in large numbers in regions where the wind potential is high. When the wind turbines work simultaneously, the grid may not be able to carry the produced electricity and hence forced to shut down (like the problem in Tamil Nadu, India). All things considered, we believe that the hydrogen storage system should be examined for each case study separately according to energy and economic analysis. The payback period was selected as economic criteria to investigate the hybrid system from economic point of view. Figure 20 illustrates the payback time of the hybrid system with different interest rates (1-7%) in the study region. It can be observed that a significant economic conclusion has been achieved for the proposed hybrid system, as the payback time of this system is ascertained at around 8 years (with the interest rate of 3%). For this calculation, the purchased grid electricity is considered to be 0.28 $/kWh.

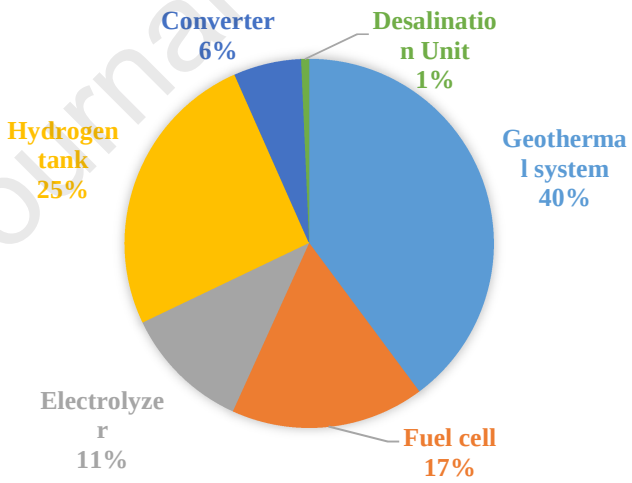

Fig. 19. The initial investment of the components.

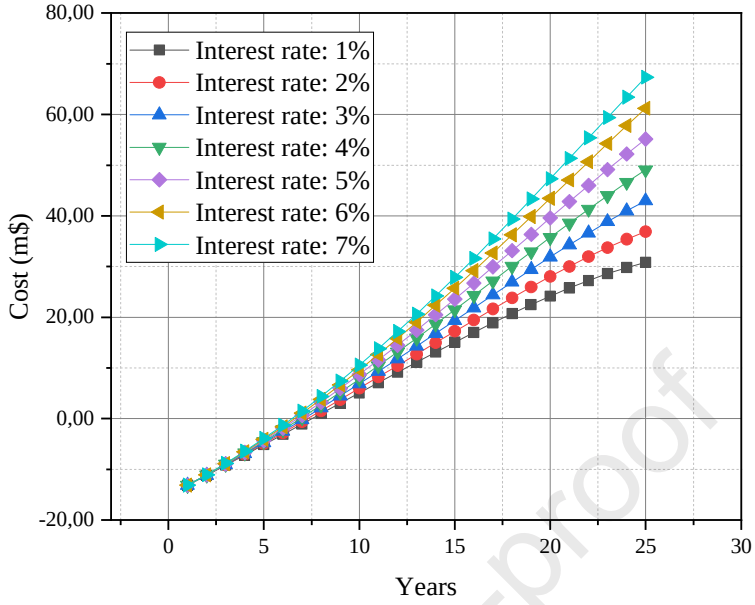

Fig. 20. Payback period of the system with various interest rate for the study region.

5. Conclusions

For energy systems based-geothermal, the low well operating lifetime and low well temperature are the main challenges. These obstacles can be covered or at least decrease by utilizing solar thermal collector before the turbine. Because of two reasons solar thermal collectors can be employed before the turbine: first, increasing the entrance enthalpy (that was investigated in the current study), and second, using instead of GE resource as long as solar energy is existence (in this case, the well operating lifetime is amplified). In the real conditions and for complicated energy systems, finding the optimum operating conditions and design parameters needs many experimental tests and intricate mathematical modeling. In this study, we proposed intelligent models based-AI to meet the need. The intelligent methods exert the input parameters to predict the targets. Hence, this capability provides a strong control option for the hybrid system by considering a wide range of input variables. Another challenge concerning GE systems is improving system efficiency. This study proposed a novel design to recover a portion of waste heat for producing freshwater. Another limitation for RESs is uncertainty in energy supply for remote area regions. We technically examined the role of the hydrogen storage system for the proposed energy system, which makes it appropriate for remoteness regions. Generally speaking, this study endeavored to cover some limitations regarding GE systems. The following conclusions have been achieved from this study:

- For modeling of the power generation, the statistical indicators have shown that MLP-ICA works better than MLP-GA in terms of R_{train}= 0.9965, R_{test}=0.9944, $RMSE_{train}$=1.5812 (kW) and $RMSE_{test}$=2.2390 (kW). The results demonstrated that enhancing the solar radiation and cooling water temperature difference, and decreasing the environment and condensing temperatures enhances the produced power of the system.

- For modeling of COP of the refrigeration system, MLP-ICA has shown a good ability to predict the COP by different input parameters. The statistical metrics for this prediction was obtained as R_{train}= 0.9969, R_{test}=0.9982, $RMSE_{train}$=0.0023 and $RMSE_{test}$=0.0014. This modeling has shown that increasing the evaporation temperature and decreasing the pinch-point and environment temperatures rise the $COP_{chiller}$.
- For modeling of the total HXA of the hybrid system, MLP-ICA has depicted higher performance prediction than MLP-GA with R_{train}= 0.9933, R_{test}=0.9936, $RMSE_{train}$=4.7362 m^2, and $RMSE_{test}$=4.3069 m^2. The effect of input variables on the total HXA have shown that increasing the solar radiation, cooling water temperature difference, evaporation temperature rises the total HXA and increasing the pinch-point temperature, environment temperature and condensing temperature declines the total HXA.
- The best statistical metrics for prediction of cycle thermal efficiency were obtained by MLP-ICA as R_{train}= 0.9958, R_{test}=0.9955, $RMSE_{train}$=2.4314e-04 and $RMSE_{test}$=1.9131e-04. It was observed that increasing the solar irradiance and cooling water temperature difference, and decreasing environment and condensing temperatures increases the cycle thermal efficiency.
- Using the waste heat of ARS condenser, can run a 10,000 kJ/m^3 desalination unit by which 3.2 m^3/h sweet water is produced. Also, it was concluded that the COP of ARS significantly increases by employing the desalination unit.
- The payback period of the hybrid system in the study region (by considering the interest rate of 3%) was obtained to be around 8 years.

Future works: The proposed system can be examined by considering a compressed air energy storage system (CAES) as a substitute for the hydrogen storage system. Also, considering a biomass energy resource instead of the geothermal resource would be interesting for the proposed system. Moreover, by increasing the size of the storage system, the proposed system can be exerted in a hybrid system incorporating with wind turbines to supply the energy demand for a larger case study.

Acknowledgement
The authors acknowledge the financial support of Aalto University (Grant no. Post doc/T21201) for this research.

References

[1] "Global Warming of 1.5 °C." [Online]. Available: https://www.ipcc.ch/sr15/. [Accessed: 21-Jan-2019].

[2] A. Khosravi, S. Syri, X. Zhao, and M. E. H. Assad, "An artificial intelligence approach for thermodynamic modeling of geothermal based-organic Rankine cycle equipped with solar system," *Geothermics*, vol. 80, pp. 138–154, 2019.

[3] Y. Chang, Y. Gu, L. Zhang, C. Wu, and L. Liang, "Energy and environmental implications of using geothermal heat pumps in buildings: An example from north China," *J. Clean. Prod.*, vol. 167, pp. 484–492, 2017.

[4] Q. Zhang, S. Chen, Z. Tan, T. Zhang, and B. Mclellan, "Investment strategy of hydrothermal geothermal heating in China under policy, technology and geology uncertainties," *J. Clean. Prod.*, vol. 207, pp. 17–29, 2019.

[5] C. Coskun, Z. Oktay, and I. Dincer, "Thermodynamic analyses and case studies of geothermal based multi-generation systems," *J. Clean. Prod.*, vol. 32, pp. 71–80, 2012.

[6] A. Hmida, N. Chekir, A. Laafer, M. E. A. Slimani, and A. Ben Brahim, "Modeling of cold room driven by an absorption refrigerator in the south of Tunisia: A detailed energy and thermodynamic analysis," *J. Clean. Prod.*, vol. 211, pp. 1239–1249, 2019.

[7] D. Zurmuhl, M. Lukawski, G. Aguirrer, W. Law, G. Schnaars, K. Beckers, C. Anderson, J. Tester "Hybrid geothermal heat pumps for cooling telecommunications data centers," *Energy Build.*, vol. 188–189, pp. 120–128, 2019.

[8] T. Bao, J. Meldrum, C. Green, S. Vitton, Z. Liu, and K. Bird, "Geothermal energy recovery from deep flooded copper mines for heating," *Energy Convers. Manag.*, vol. 183, pp. 604–616, 2019.

[9] M. Moosavi and N. Soltani, "Prediction of hydrocarbon densities using an artificial neural network-group contribution method up to high temperatures and pressures," *Thermochim. Acta*, vol. 556, pp. 89–96, 2013.

[10] W. F. He, D. Han, and T. Wen, "Energy, entropy and cost analysis of a combined power and water system with cascade utilization of geothermal energy," *Energy Convers. Manag.*, vol. 174, pp. 719–729, 2018.

[11] X. Zhang, X. Liu, X. Sun, C. Jiang, H. Li, Q. Song, J. Zeng, G. Zhang, "Thermodynamic and economic assessment of a novel CCHP integrated system taking biomass, natural gas and geothermal energy as co-feeds," *Energy Convers. Manag.*, vol. 172, pp. 105–118, 2018.

[12] Y. E. Yuksel, M. Ozturk, and I. Dincer, "Thermodynamic analysis and assessment of a novel integrated geothermal energy-based system for hydrogen production and storage," *Int. J. Hydrogen Energy*, vol. 43, no. 9, pp. 4233–4243, 2018.

[13] B. Tomaszewska, L. Pająk, J. Bundschuh, and W. Bujakowski, "Low-enthalpy geothermal energy as a source of energy and integrated freshwater production in inland areas: Technological and economic feasibility," *Desalination*, vol. 435, pp. 35–44, 2018.

[14] G. Falcone, X. Liu, R. R. Okech, F. Seyidov, and C. Teodoriu, "Assessment of deep geothermal energy exploitation methods: The need for novel single-well solutions," *Energy*, vol. 160, pp. 54–63, 2018.

[15] K. Salhi, M. Korichi, and K. M. Ramadan, "Thermodynamic and thermo-economic analysis of compression–absorption cascade refrigeration system using low-GWP HFO refrigerant powered by geothermal energy," *Int. J. Refrig.*, vol. 94, pp. 214–229, 2018.

[16] Tesha, "Absorption Refrigeration System as an Integrated Condenser Cooling Unit in Geothermal," 2009.

[17] W. F. He, H. X. Yang, and D. Han, "Thermodynamic analysis of a power and water combined system with geothermal energy utilization," *Geothermics*, vol. 76, pp. 106–115, 2018.

[18] G. Yu and Z. Yu, "Investigation of Geothermally Sourced Combined Power and Freshwater Generation Systems," *Energy Procedia*, vol. 158, pp. 5946–5953, 2019.

[19] A. Khosravi, R. N. N. Koury, L. Machado, and J. J. G. Pabon, "Energy, exergy and economic analysis of a hybrid renewable energy with hydrogen storage system," *Energy*, vol. 148, no. C, pp. 1087–1102, 2018.

[20] A. Khosravi, S. Syri, M. El Haj Assad, and M. Malekan, "Thermodynamic and Economic Analysis of a Hybrid Ocean Thermal Energy Conversion/Photovoltaic System with Hydrogen-Based Energy Storage System," *Energy*, vol. 172, pp. 304–319, 2019.

[21] F. Rodríguez, A. Fleetwood, A. Galarza, and L. Fontán, "Predicting solar energy generation through artificial neural networks using weather forecasts for microgrid control," *Renew. Energy*, vol. 126, pp. 855–864, 2018.

[22] R. A. Conde-Gutiérrez, U. Cruz-Jacobo, A. Huicochea, S. R. Casolco, and J. A. Hernández, "Optimal multivariable conditions in the operation of an absorption heat transformer with energy recycling solved by the genetic algorithm in artificial neural network inverse," *Appl. Soft Comput.*, vol. 72, pp. 218–234, 2018.

[23] F. Martellotta, U. Ayr, P. Stefanizzi, A. Sacchetti, and G. Riganti, “On the use of artificial neural networks to model household energy consumptions,” *Energy Procedia*, vol. 126, pp. 250–257, 2017.

[24] A. Khosravi, R. N. N. Koury, L. Machado, and J. J. G. Pabon, “Prediction of wind speed and wind direction using artificial neural network, support vector regression and adaptive neuro-fuzzy inference system,” *Sustain. Energy Technol. Assessments*, vol. 25, pp. 146–160, 2018.

[25] A. Khosravi, L. Machado, and R. N. Oliviera, “Time-series prediction of wind speed using machine learning algorithms: A case study Osorio wind farm, Brazil,” *Appl. Energy*, vol. 224, no. C, pp. 550–566, 2018.

[26] A. Khosravi, R. O. Nunes, M. E. H. Assad, and L. Machado, “Comparison of artificial intelligence methods in estimation of daily global solar radiation,” *J. Clean. Prod.*, vol. 194, pp. 342–358, 2018.

[27] A. Khosravi, R. N. N. Koury, L. Machado, and J. J. G. Pabon, “Prediction of hourly solar radiation in Abu Musa Island using machine learning algorithms,” *J. Clean. Prod.*, vol. 176, no. C, pp. 63–75, 2018.

[28] D.-S. Kim, “Solar Absorption Cooling,” Delft University of Technology, 2007.

[29] “System Advisor Model (SAM) |.” [Online]. Available: https://sam.nrel.gov/. [Accessed: 13-Mar-2019].

[30] E. Atashpaz-Gargari and C. Lucas, “Imperialist competitive algorithm: An algorithm for optimization inspired by imperialistic competition,” in *2007 IEEE Congress on Evolutionary Computation*, 2007, pp. 4661–4667.

[31] “Renewables.ninja.” [Online]. Available: https://www.renewables.ninja/. [Accessed: 09-Jul-2019].

[32] Y. Noorollahi, H. Yousefi, R. Itoi, and S. Ehara, “Geothermal energy resources and development in Iran,” *Renew. Sustain. Energy Rev.*, vol. 13, no. 5, pp. 1127–1132, 2009.

[33] A. Saffarzadeh and Y. Noorollahi, “Geothermal Development in Iran: A Country Update,” in *Proceedings World Geothermal Congress 2005*, 2005.

[34] A. Keçeciler, H. İ. Acar, and A. Doğan, “Thermodynamic analysis of the absorption refrigeration system with geothermal energy: An experimental study,” *Energy Convers. Manag.*, vol. 41, no. 1, pp. 37–48, 2000.

[35] Tesha, “Absorption refrigeration system as an integrated condenser cooling unit in a geothermal power plant,” in *Proceedings World Geothermal Congress 2010*, 2010.

Highlights

- A hybrid system based on geothermal energy combined with solar system was designed
- Desalination unit and hydrogen storage system were integrated into the geothermal system
- MLP-ICA and MLP-GA were developed to simulate the behavior of the hybrid system
- MLP-ICA operates better than the MLP-GA for modeling the hybrid system
- The payback time of the hybrid system with the interest rate of 3% is around 8 years

Declaration of interests

☒ The authors declare that they have no known competing financial interests or personal relationships that could have appeared to influence the work reported in this paper.

☐The authors declare the following financial interests/personal relationships which may be considered as potential competing interests:

Ali Khosravi

Sanna Syri